Onboard tuning of vessel seakeeping model parameters and sea state characteristics

Xu Han *, Bernt Johan Leira, Svein Sævik, Zhengru Ren

Department of Marine Technology, Norwegian University of Science and Technology (NTNU), 7491 Trondheim, Norway
Centre for Research-based Innovation on Marine Operations (SFI MOVE), Norway

ARTICLE INFO

ABSTRACT

It is essential for a safe and cost-efficient marine operation to improve the knowledge about the real-time onboard vessel conditions. This paper proposes a novel algorithm for simultaneous tuning of important vessel seakeeping model parameters and sea state characteristics based on onboard vessel motion measurements and available wave data. The proposed algorithm is fundamentally based on the unscented transformation and inspired by the scaled unscented Kalman filter, which is very computationally efficient for large dimensional and nonlinear problems. The algorithm is demonstrated by case studies based on numerical simulations, considering realistic sensor noises and wave data uncertainties. Both long-crested and short-crested wave conditions are considered in the case studies. The system state of the proposed tuning framework consists of a vessel state vector and a sea state vector. The tuning results reasonably approach the true values of the considered uncertain vessel parameters and sea state characteristics, with reduced uncertainties. The quantification of the system state uncertainties helps to close a critical gap towards achieving reliability-based marine operations.

1. Introduction

For marine operations, operational limit diagrams are normally provided in operating reports or operation manual booklets. Normally, there are many variables that influence these diagrams, such as vessel heading, loading condition, vessel speed, water depth, wave condition, and operation phase, so that dimension reduction must be considered as a compromise with readability. As a result, conservatism is typically increased. By means of IT tools and increased onboard communicating and computing capacity, real-time and interactively updated operational limit diagrams can be available without sacrificing useful information and knowledge.

It is also well recognized that the vessel operational conditions (defined by vessel inertia distribution, damping, forward speed, and the encountered weather and water depth conditions) are always subject to uncertainties [1], and those uncertain parameters can significantly influence the resulting vessel motion estimation [1–3]. A successful onboard decision support system (ODSS) for operation optimization and risk avoidance normally requires accurate real-time vessel motion prediction. For decades, there has been a strong research interest in relation to wave-induced vessel motion prediction in real time. Without wave prediction, one is still able to predict vessel motions by extrapolation of the recorded motion time series based on various approaches. Li et al. [4] qualitatively compared different typical predictive models within the machine learning domain. In general, the applicable predictive models for nonlinear time series involving machine learning could (1) be too computationally expensive to use online (e.g., support vector machine [5], fuzzy logic, and decision tree methods); (2) require highly customized modeling (e.g., wavelet neural network [6]); (3)

---

* Corresponding author at: Department of Marine Technology, Norwegian University of Science and Technology (NTNU), 7491 Trondheim, Norway.
E-mail address: xu.han@ntnu.no (X. Han).

Nomenclature

$\%\Delta\sigma_A^2$	The variance reduction for parameter A due to tuning. A can be H_s, T_p, β_W, etc.
α	Scaling factor for the UKF model
$\bar{x}_j$	The mean value of the filtered sensor signal $\hat{x}_j(t)$
β	Hyperparameter in the UKF model in order to partially account for higher order statistical properties
β_{44}	Ratio between the additional roll damping and the critical roll damping
β_{Wp}	The prevailing wave direction for short-crested waves
β_W	Wave direction w.r.t. vessel coordinate system
$\bar{\boldsymbol{P}}_k$	The state covariance matrix for $\bar{\boldsymbol{x}}_k$
$\bar{\boldsymbol{x}}_k$	The predicted system state for the kth update
$\boldsymbol{\mathcal{X}}_{k,i}^{\phi}$	The vessel state for the sigma point $\boldsymbol{\mathcal{X}}_{k,i}$
$\boldsymbol{\mathcal{X}}_{k,i}^{\theta}$	The sea state for the sigma point $\boldsymbol{\mathcal{X}}_{k,i}$
$\boldsymbol{\mathcal{X}}_{k,i}$	The ith sigma point for the system state $\boldsymbol{x}_k$, i.e., the ith column of $\boldsymbol{\mathcal{X}}_k$
$\boldsymbol{\mathcal{X}}_k$	The sigma points for the system state $\boldsymbol{x}_k$
$\bar{\boldsymbol{\mathcal{Z}}}_k$	The predicted measurement vector estimated based on all sigma points
$\boldsymbol{\phi}_k$	The vessel state after the kth update
θ_k'	The acquired sea state information for the kth update
θ_k	The sea state after the kth update
$\boldsymbol{K}$	Kalman gain
$\boldsymbol{P}_k^w$	The covariance matrix for $\boldsymbol{x}_k^w$
$\boldsymbol{P}_{\theta_k}'$	The prior uncertainty of θ_k'
$\boldsymbol{P}_k$	The system state covariance matrix for $\boldsymbol{x}_k$
$\boldsymbol{P}_{\phi_k}$	The covariance matrix for $\boldsymbol{\phi}_k$
$\boldsymbol{P}_{\theta_k}$	The covariance matrix for θ_k
$\boldsymbol{P}_{xz_k}$	The cross covariance matrix for the system state in state space and measurement space at kth measurement update step
$\boldsymbol{P}_{z_k}$	The covariance matrix for the system state in measurement space at kth measurement update step
$\boldsymbol{Q}$	Process uncertainty covariance matrix
$\boldsymbol{R}$	Measurement uncertainty covariance matrix
$\boldsymbol{v}$	Process disturbance
$\boldsymbol{x}_k^w$	The system state after weather update step for the kth sea state
$\boldsymbol{x}_k$	The system state after the kth update
$\boldsymbol{y}_k$	The residual at kth measurement update step
$\boldsymbol{Z}_{k,i}$	The predicted measurement vector at $\boldsymbol{\mathcal{X}}_{k,i}$, built based on all sensor signals $x_j(t)$, for $j = 1, 2, \ldots, J$
$\boldsymbol{z}_k$	The acquired measurements at the kth update step (i.e., the standard deviations of sensor signals)
$\Delta\hat{A}$	The error between the true and the tuned values for parameter A. A can be H_s, T_p, β_W, etc.
$\eta_3, \dot{\eta}_3, \ddot{\eta}_3$	Heave displacement, velocity, acceleration
$\hat{\sigma}_A$	The standard deviation of the tuned parameter A. A can be H_s, T_p, β_W, etc.
$\hat{\sigma}_j$	The standard deviation of the filtered signal $\hat{x}_j(t)$
$\hat{A}$	The tuned value of parameter A. A can be H_s, T_p, β_W, etc.
$\hat{x}_j(t)$	The filtered time series for sensor signal $x_j(t)$
κ	Hyperparameter in the UKF model
ω	Wave frequency
$\bar{\sigma}_A$	The standard deviation of the acquired parameter A. A can be H_s, T_p, β_W, etc.
$\bar{A}$	The acquired value of parameter A. A can be H_s, T_p, β_W, etc.
ψ	Phase angle between the wave elevation and the vessel response in the RAO
σ_N^2	Variance of signal noise
σ_A	The standard deviation of the random variable A. A can be H_s, T_p, β_W, β_{44}, XCG, etc.
$\sigma_{j,i}$	The predicted measurement (response standard deviation) corresponding to the sensor measurement $x_j(t)$ based on the sigma point $\boldsymbol{\mathcal{X}}_{k,i}$
τ	Initial seed for case simulations

and lack of physical reasoning. Despite the complexity and computational cost, purely machine learning based predictive models such as neural network in general do not outperform compared with other classical prediction methods such as autoregressive models and minor component analysis [7]. Nielsen et al. [8] proposed a ship motion prediction algorithm based on the autocorrelation

ε_A	The error between the true and the acquired values for parameter A. A can be H_s, T_p, β_W, etc. $\varepsilon_A = \Delta\overline{A}$
φ	Random phase angle for wave components
A^*	The true value of parameter A. A can be H_s, T_p, β_W, etc.
f_{lp}	Lowpass filter cutoff frequency [Hz]
$H_j(\omega, \beta_W | \mathcal{X}_{k,i})$	The RAO corresponding to the system state $\mathcal{X}_{k,i}$ and the sensor signal $x_j(t)$
H_s	Significant wave height
J	The total number of sensor measurements for one sea state
j	Sensor ID, the jth sensor measurement, representing different quantities (displacement, velocity, acceleration) and locations
k	The sea state number
N	The dimension of the system state
n_s	Spreading parameter for short-crested waves
N_t	Number of time steps for the sensor signals
N_{β_W}	Number of discrete directions for each spectrum
N_ω	Number of discrete frequencies for each 1D spectrum
$S^*_{X_j X_j}(\omega)$	The true vessel motion spectrum for sensor j
$S_{\zeta\zeta}(\omega, \beta_W | \mathcal{X}^\theta_{k,i})$	The single-sided wave spectrum corresponding to the sea state $\mathcal{X}^\theta_{k,i}$
$S_{\zeta\zeta}(\omega, \beta_W)$	Single-sided wave spectrum
$S_{j,i}(\omega)$	The estimated vessel motion spectrum based on the sigma point $\mathcal{X}^\theta_{k,i}$ corresponding to the signal $x_j(x)$
T_p	Wave spectral peak period
w^c_i	The weight factor for state mean calculation at the ith sigma point, $i = 0, 1, 2, \ldots, 2N$
w^m_i	The weight factor for state covariance calculation at the ith sigma point, $i = 0, 1, 2, \ldots, 2N$
$x_j(t)$	The original signal for the jth sensor measurement for a certain sea state
DP	Dynamic positioning
ODSS	Onboard decision support system
OSV	Offshore supply vessel
PM	Pierson–Moskowitz spectrum
RAO	Response amplitude operator
SNR	Signal-to-noise ratio
UKF	Unscented Kalman filter
WMO	World Meteorological Organization
XCG	Longitudinal coordinate of vessel center of gravity

function of the measured motion time series. Due to the highly random nature of the encountered waves, it is challenging to ensure the time series extrapolation quality. The algorithms mentioned above reported reliable predictions of wave-induced vessel motions from a few seconds up to less than a minute ahead.

Alternatively, the wave-induced vessel motion can be predicted by seakeeping analysis based on wave forecast and predefined vessel conditions, without taking advantage of historical motion records. Seakeeping analysis has been commonly applied for design of floaters and floater-involved marine operations [9]. Usually transfer functions between vessel motions and wave elevations from seakeeping analysis can be linearized [10] and applied for real-time motion prediction. The corresponding prediction capacity is limited by the accuracy of the wave forecast and the applied linear transfer functions, i.e., response amplitude operators (RAOs). In recent decades, research about ODSS has been mainly focused on improving vessel motion prediction by improving the wave prediction for the near future by: (1) processing of coherent wave radar signals [11,12]; (2) using non-coherent wave radar signals combined with ship motion measurements [13–15]; (3) applying "ship as a wave buoy" analogy [16,17] assuming stationary sea states and predicting the future sea state by extrapolation; (4) or improving the accuracy of the wave analysis model [18–20].

Although seldom addressed, it is equally important to quantify and reduce the uncertainties associated with vessel seakeeping model parameters for a risk-based ODSS [1]. Practically, the uncertainties of vessel parameters for marine operations can be reduced by (1) careful design and organization of marine operation activities; (2) directly using available vessel condition monitoring systems such as the ballasting system and draft measurement. However, important vessel parameters related to inertia distribution and damping are challenging to measure directly and still expected to be subject to significant uncertainties. Identification of these important vessel hydrodynamic parameters has been mainly studied for maneuvering [21–23] and dynamic positioning (DP) [24] scenarios, where the responses at wave frequencies are considered as a disturbance or simply ignored. The estimated hydrodynamic coefficients such as added mass and damping may be questionable to apply for future wave conditions. Compared with tuning DP and maneuvering models, seakeeping model tuning is even more challenging because it must explicitly consider the highly variable wave loads.

Han et al. [25] proposed a promising online algorithm to improve the knowledge about the important vessel parameters and quantify the uncertainties, based on onboard vessel motion measurements and wave information (in terms of wave spectrum). The algorithm is based on discrete Bayesian inference and the tuned parameters can improve the accuracy of the RAOs to be applied for future sea states. Roll motion is subject to high nonlinearity due to the significant influence from nonlinear roll damping sources such as eddy making and bilge keel induced damping [26]. Such damping terms are defined as "additional" damping, differing from the damping derived from the linear potential theory. However in practice, such additional roll damping is usually linearized at each sea state by e.g., stochastic linearization [27] so that the roll motion transfer function can represent a linear behavior. As a consequence, the additional roll damping becomes sea state dependent. Han et al. [28] proposed two procedures for tuning and predicting such sea state dependent parameters together with other vessel parameters.

However, the algorithm of vessel seakeeping model tuning is still at an early developing stage with many identified challenges towards industrial applications. The acquired wave information can never be exact. Precise knowledge about the wave spectrum was assumed in the previous research [25,28]. The feasibility of the previously proposed tuning algorithms with Bayesian inference technique have been demonstrated, by considering up to 4 uncertain vessel parameters. In reality, more uncertain parameters should be included in the tuning model, e.g., vessel heading and speed, wave spectrum related parameters such as H_s (significant wave height), T_p (wave spectral peak period), β_W (wave direction), directional spreading, and many other hydrodynamic parameters. As a consequence, the previously developed methodology faces a common challenge with respect to the curse of dimensionality [29]. This makes the discrete Bayesian inference based model tuning approach time-consuming, computationally expensive, and hence unrealistic for practical applications within such an extended system framework.

To solve the curse of dimensionality, this paper proposes a novel and much more efficient algorithm to tune the vessel seakeeping model parameters by applying a second-order statistical inference algorithm based on the mean and variance of the variables. The newly proposed algorithm also considers the uncertainties from waves and can even reduce these uncertainties through the proposed tuning procedure. The paper is organized as follows. The uncertainties from wave information are discussed in Section 2. Then the new tuning algorithm is described in Section 3. The proposed algorithm is demonstrated numerically by case studies. The basis of the considered seakeeping model, generation of synthetic sensor signals, and the base case inputs are described in Section 4. The results of the base case and associated sensitivity studies are presented in Section 5. Finally, Section 6 summarizes the main findings from the present study and gives suggestions for future work.

2. Wave data and the associated uncertainties

Wave field data can be collected through forecast, hindcast, visual observation, or instrumental measurements, among which the measurements by instruments such as wave buoys, shipborne wave recorders, satellite altimeters, and onboard radars may be subject to minimum error. Practically, any type of wave data can be valuable for tuning of the seakeeping model parameters.

Nowadays wave forecast and hindcast mostly use the third-generation wave models, e.g., WAM, accounting for the nonlinear interaction between wave components [30]. The uncertainty of wave forecast may be well quantified by the spread of the wave ensemble prediction [31,32]. The wave forecast could be biased, especially in sheltered or coastal areas. Natskår et al. [33] compared the wave data between forecast and hindcast. Biased H_s was observed in the forecast data.

The comparison study by Orimolade et al. [34] indicates that (1) the wave forecast uncertainty also depends on the location to be forecasted; (2) and the instrumental error of the MIROS microwave radar onboard the Heidrun platform may be generally higher than the wave buoy measurements used for Barents Sea. Comparisons between summer and winter seas [34] may suggest that the wave information obtained by wave radar measurements performed in a more stable way across mild and harsh seas, even with relatively large measuring errors. The measurement errors by wave buoys are much smaller at moderate seas but can be significantly increased at harsh environmental conditions. Hagen et al. [35] also argued that breaking waves or slamming acting on a wave buoy may lead to overestimation of wave heights, while underestimation may occur for severe seas due to the buoy being drawn through the wave crest, or for large surface current.

To assure a globally aligned measurement quality, the World Meteorological Organization (WMO) has published recommendations and requirements for instrument performance [36]. The specified measurement uncertainties corresponds to a 95% probability level, i.e., two standard deviations (2σ) for a Gaussian distribution. The measurements should, where possible, record the sea state characteristics (e.g., H_s, T_p, and β_W) for wind sea and swell, separately.

Please note that the specified uncertainties of the WaMoSII system and the WAM results are only based on the available indicative accuracy information [1,37]. It is assumed that the accuracy approximately corresponds to a 95% confidence level. The term "accuracy" is less preferred compared with "uncertainty" [36] because "accuracy" can be determined only when the true value is perfectly known. Natskår et al. [33] reported even higher uncertainties on the forecast T_p, in comparison with hindcast wave data.

The freely accessible ERA5 datasets [38] and toolbox provide comprehensive opportunities of reanalyzing wave data both in terms of the expectation and the uncertainty assessment, based on the Integrated Forecasting System (IFS) Cy41r2 which combines WAM forecast and available observations. However, it is worth noting that ERA5 mostly considers random errors in terms of ensemble spread [32] but not systematic errors. The uncertainties of the ERA5 datasets are highly dependent on the amount and quality of available observations, resolution, location, and season. The wave analysis results and their uncertainty assessment may be biased, due to the potential systematic errors, e.g., in the cases of tropical and extra-tropical cyclones. By benefiting from the development of the wave model [30], data assimilation [39], and observation handling [40], the uncertainties of the ocean wave analysis in terms of both bias and variance have been significantly reduced [20].

Table 1
Operational measurement uncertainties (2σ) [36].

Variable	H_s	T_p	β_W
WMO required[a]	0.5 m for $H_s \leq 5$ m; 10% for $H_s > 5$ m	0.5 s	10°
WMO achievable[b]	0.5 m for $H_s \leq 5$ m; 10% for $H_s > 5$ m	0.5 s	20°
Typical moored buoy	0.2 m or 10%	1.0 s	10°
WaMoSII radar [1,37]	0.5 m or 10%	0.5 s	2°
Wave model (WAM) [1]	0.5 m or 15%	10%	15°

[a]"WMO required" corresponds to the recommended requirements about the measurement uncertainty for general operational use [36].
[b]"WMO achievable" corresponds to the realistic measurement uncertainty that the sensor can be achieved in normal operational practice [36].

Table 2
Applied uncertainties of the measured sea state characteristics.

Variable	Standard deviation	Unit
H_s	10%	m
T_p	0.5	s
β_W	5	°

The wave information used in the state estimation model should include uncertainties from instrumental sensors, sampling variability (e.g., due to discrete measured data with limited duration for a relatively large recording interval), temporal and spatial variability (i.e., using the imperfectly synchronized measurement data from another location), and inaccurate description of waves caused by e.g., the selection of wave models and probability distribution models. However, in reality the mentioned uncertainties are very challenging to quantify and estimate independently. The reported uncertainties from sampling variability and temporal and spatial variability by Bitner-Gregersen and Hagen [41] are well within the WMO required measurement accuracy. Therefore, it is rational to consider that the specified measurement uncertainties in Table 1 have included the sampling, temporal, and spatial variability to some degree. Due to the sampling variation, the Joint Committee on Structural Safety suggests longer wave recording length (even with less accuracy) for each recording interval rather than too short wave records within each interval (even with high accuracy) [35].

Based on the discussion above, the considered uncertainties of sea state characteristics are summarized in Table 2, assuming that the sea state information is from measurements or hindcast. A sensitivity case considering larger uncertainties was also carried out, see Section 5.4.

The long-term distribution of T_p is normally modeled as conditional upon H_s with a log-normal distribution [42]. However, the short-term distribution of T_p with a prior knowledge with respect to H_s and T_p from measurements, hindcast, or forecast can be reasonably approximated as being Gaussian distributed, i.e., $P(T_p | \overline{H}_s, \overline{T}_p) \sim \mathcal{N}(\overline{T}_p, \overline{\sigma}_{T_p}^2)$, where $\overline{H}_s$ and $\overline{T}_p$ represent the prior, and $\overline{\sigma}_{T_p}^2$ represents the uncertainties (variance) of the prior $\overline{T}_p$.

3. Formulation of algorithm

Real applications of vessel seakeeping model tuning must consider many uncertain sea state characteristics as described in Section 2, as well as a large number of uncertain vessel parameters. Consequently, the curse of dimensionality from the previously proposed discrete Bayesian inference approach [25] must be overcome for practical applications. The most common practice is to approximate the joint probability distribution of the random variables by taking account of their properties related to the first two orders, i.e., the mean vector and the covariance matrix, and assuming the variables are multivariate Gaussian distributed. The Kalman filter and its extended forms are the most popular algorithms updating the assumed Gaussian distributed state based on measurements. Tuning of vessel seakeeping parameters is a multi-dimensional, multi-modal and nonlinear problem [25]. As shown later, it is difficult to express the measurement function from the system state (including vessel parameters and sea state characteristics) to the measurement (i.e., the standard deviation of vessel motion) in an algebraic format. Comparing the performance among the popular nonlinear Kalman filters [43–47], the unscented Kalman filter (UKF) [46] is found to be relatively feasible for the seakeeping model tuning problem, with respect to estimation accuracy, implementation convenience, numerical robustness, and computational expense. UKF is formulated based on the unscented transformation [48] directly through nonlinear functions.

The proposed tuning algorithm is then based on the UKF model, consisting of four steps: weather update, sigma-point and weight calculation, system propagation, and measurement update. Different from the typical UKF models which update the state of the dynamic system for each time instant, the proposed UKF model updates the system state for each sea state, assuming that the system state is approximately stationary during each sea state. The tuning procedure is illustrated in Fig. 1. Details are described in the following sections.
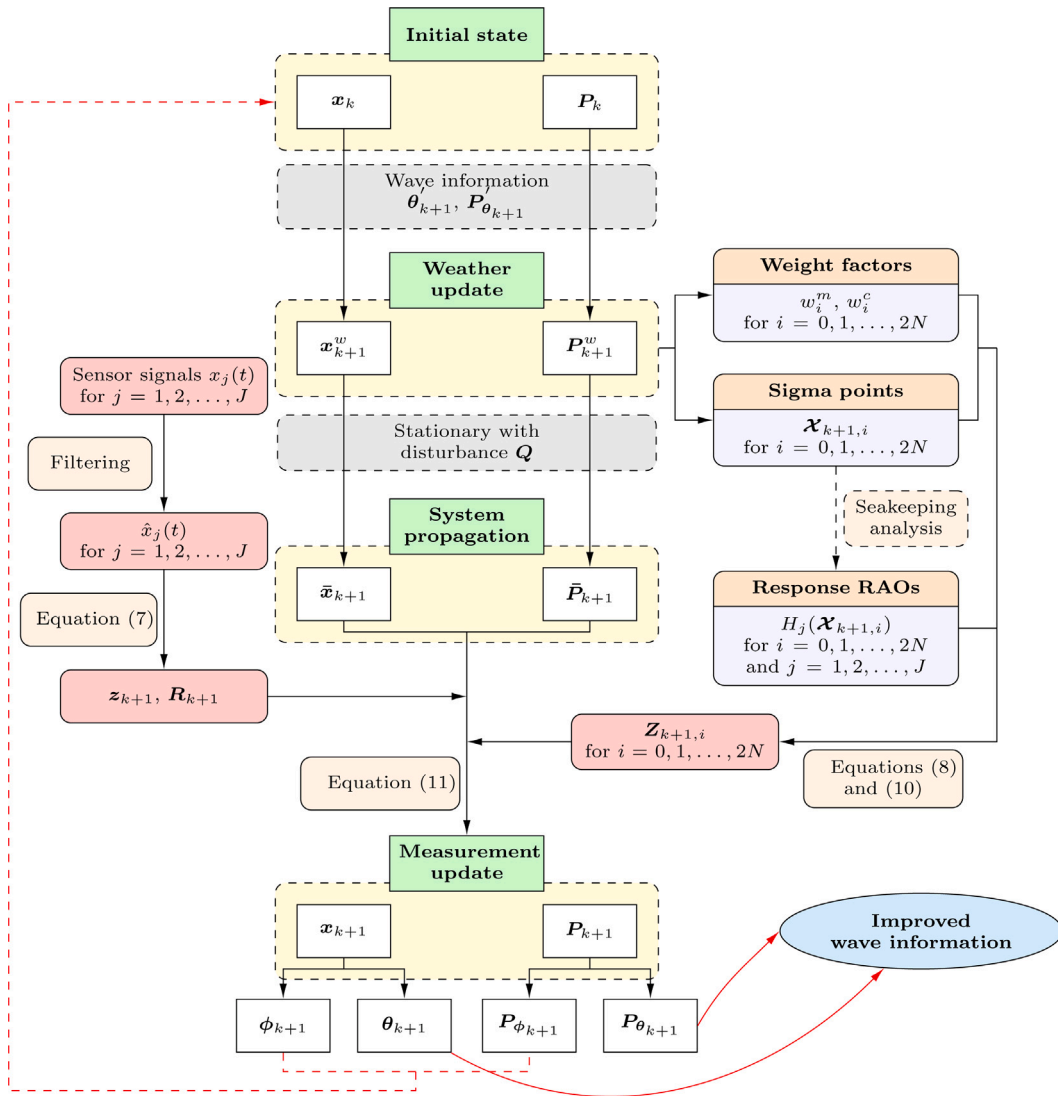
Fig. 1. The process of tuning vessel parameters and sea state characteristics together with quantification of uncertainties.

3.1. Weather update

The system state $\boldsymbol{x}_k$ at the sea state indexed by k consists of a vessel state $\boldsymbol{\phi}_k$ including uncertain vessel parameters and a sea state $\boldsymbol{\theta}_k$ including uncertain sea state characteristics such as H_s, T_p, and β_W. The subscript k indicates the corresponding parameter that has been tuned for k sea states. Wave conditions can be considered stationary within a sea state. Normally a stationary sea state can last from 20 min up to 3 h, depending on the location. $\boldsymbol{\phi}_k$ and $\boldsymbol{\theta}_k$ are approximately constant within that sea state. For the next sea state with the acquired wave information $\boldsymbol{\theta}'_{k+1}$ and its uncertainty $\boldsymbol{P}'_{\theta_{k+1}}$, the system state should be updated accordingly. This step is referred to as weather update:

$$\boldsymbol{x}^w_{k+1} = \begin{bmatrix} \boldsymbol{\phi}_k \\ \boldsymbol{\theta}'_{k+1} \end{bmatrix} \tag{1a}$$

$$\boldsymbol{P}^w_{k+1} = \begin{bmatrix} \boldsymbol{P}_{\phi_k} & \boldsymbol{0} \\ \boldsymbol{0} & \boldsymbol{P}'_{\theta_{k+1}} \end{bmatrix} \tag{1b}$$

where the superscript w means the corresponding variable after the weather update step. Compared with the state after the kth update i.e., $\boldsymbol{x}_k$ and $\boldsymbol{P}_k$, the sub-variables $\boldsymbol{\theta}_k$ and $\boldsymbol{P}_{\theta_k}$ have been replaced by $\boldsymbol{\theta}'_{k+1}$ and $\boldsymbol{P}'_{\theta_{k+1}}$ respectively. In addition, the off-diagonal sub-matrices $\boldsymbol{P}_{\phi_k\theta_k}$ and $\boldsymbol{P}_{\theta_k\phi_k}$ are replaced by zeros.

3.2. Calculation of sigma points and weight factors

The sigma points $\mathcal{X}_{k+1}$ in the state space are calculated by [43]

$$\mathcal{X}_{k+1,0} = x_{k+1}^w \tag{2a}$$

$$\mathcal{X}_{k+1,i} = \begin{cases} x_{k+1}^w + \left[\sqrt{(N+\lambda)P_{k+1}^w}\right]_i & \text{for } i = 1, 2, \ldots, N \\ x_{k+1}^w - \left[\sqrt{(N+\lambda)P_{k+1}^w}\right]_{i-N} & \text{for } i = N+1, \ldots, 2N \end{cases} \tag{2b}$$

$$\mathcal{X}_{k+1} = [\mathcal{X}_{k+1,0} \quad \mathcal{X}_{k+1,1} \quad \cdots \quad \mathcal{X}_{k+1,2N}] \tag{2c}$$

where $\left[\sqrt{(N+\lambda)P_{k+1}^w}\right]_i$ means the ith column (or row) of the matrix square root of $(N+\lambda)P_{k+1}^w$. N is the dimension of the system state vector. $\mathcal{X}_{k+1}$ has a size of $N \times (2N+1)$. Each sigma point $\mathcal{X}_{k+1,i}$ ($i \in \{0, 1, \ldots, 2N\}$) is a deterministically selected state vector, and it can be written as

$$\mathcal{X}_{k+1,i} = \begin{bmatrix} \mathcal{X}_{k+1,i}^\phi \\ \mathcal{X}_{k+1,i}^\theta \end{bmatrix} \tag{3}$$

where $\mathcal{X}_{k+1,i}^\phi$ and $\mathcal{X}_{k+1,i}^\theta$ are the corresponding vessel state and sea state at the sigma point $\mathcal{X}_{k+1,i}$. Coefficient λ in Eq. (2) is calculated by [43]:

$$\lambda = \alpha^2(N+\kappa) - N \tag{4}$$

where α is the so-called scaling factor, and the parameter κ can have any value as long as $N + \kappa \neq 0$, and is normally set to be $3 - N$ or 0.

The weight factors corresponding to the calculated sigma points are independent of updating step k and can be calculated by [43]:

$$w_0^m = \frac{\lambda}{\lambda + N} \tag{5a}$$

$$w_0^c = \frac{\lambda}{\lambda + N} + 1 - \alpha^2 + \beta \tag{5b}$$

$$w_i^c = w_i^m = \frac{1}{2(\lambda + N)} \tag{5c}$$

where $i = 1, 2, \ldots, 2N$. w^m are the weight factors for the state mean calculation while w^c are the weight factors for the state covariance matrix calculation. β is introduced in the scaled UKF by Julier [46] to partially include the higher order statistical information, and $\beta = 2$ for Gaussian distributed variables. To ensure a positive semi-definite covariance matrix, all the weight factors w_i^c for $i = 0, 1, \ldots, 2N$ should be non-negative [46]. Consequently, it requires (1) $\kappa > -N$; (2) and approximately $\alpha > \sqrt{\frac{N}{4(N+\kappa)}}$ assuming a relatively small α value. The criterion (2) is practically difficult to achieve because the UKF normally performs better with a very small α value such as 0.01 [46]. Julier et al. [49] proposed a modified formulation for covariance calculation in order to guarantee a positive semi-definite covariance matrix.

3.3. System propagation

The vessel state and the sea state are assumed approximately stationary during an update. Therefore, the system propagation can be formulated as

$$\bar{x}_{k+1} = x_{k+1}^w + v \tag{6a}$$

$$\bar{P}_{k+1} = P_{k+1}^w + Q \tag{6b}$$

where $\bar{x}_{k+1}$ is the predicted state, $\bar{P}_{k+1}$ is the predicted state covariance. v is a $N \times 1$ vector representing the process disturbance, and is assumed to be multivariate Gaussian processes, i.e., $v \sim \mathcal{N}(0, Q)$ where Q is the process uncertainty covariance matrix.

3.4. Measurement update

Firstly, the acquired vessel motion signals $x_j(t)$ shall be filtered to remove the low-frequency components, bias, and high-frequency noises, in order to keep only the response energy within the wave frequency domain. $j = 1, 2, \ldots, J$, where $J = 9$ in the case studies, is the number of available sensor measurements for one sea state. The filtered signal is denoted by $\hat{x}_j(t)$ for each measured quantity, e.g., displacement, velocity, or acceleration of the heave or roll motions. The standard deviations of the filtered vessel motion signals at different locations and quantities (i.e., displacement, velocity, and acceleration) are considered to constitute the measurement space, denoted by $z_{k+1} \in \mathbb{R}^J$. z_{k+1} is calculated by:

$$z_{k+1} = \begin{bmatrix} \hat{\sigma}_1 \\ \hat{\sigma}_2 \\ \vdots \\ \hat{\sigma}_J \end{bmatrix} \tag{7a}$$

$$\hat{\sigma}_j = \sqrt{\frac{\sum_{t=1}^{N_t} \left(\hat{x}_j(t) - \bar{x}_j \right)^2}{(N_t - 1)}} \tag{7b}$$

$$\bar{x}_j = \frac{\sum_{t=1}^{N_t} \hat{x}_j(t)}{N_t} \tag{7c}$$

where N_t is the total number of time steps for the sensor measurement $x_j(t)$, and $\bar{x}_j$ is the mean value of the filtered signal $\hat{x}_j(t)$.

Transferring the states (i.e., sigma points) from the state space to the measurement space involves highly nonlinear functions, and the functions depend on the states as well. The transferred states in the measurement space is called "the predicted measurements". For a specific sensor signal $x_j(t)$ ($j \in \{1, 2, \ldots, J\}$), the corresponding predicted measurement (i.e., the standard deviation) can be calculated at each selected sigma point by Eq. (8) assuming long-crested waves.

$$S_{j,i}(\omega) = |H_j(\omega, \beta_W | \mathcal{X}_{k+1,i})|^2 S_{\zeta\zeta}(\omega, \beta_W | \mathcal{X}_{k+1,i}^\theta) \tag{8a}$$

$$\sigma_{j,i} = \sqrt{\sum_{n=1}^{N_\omega} S_{j,i}(\omega_n) \cdot \Delta\omega_n} \tag{8b}$$

where $H_j(\omega, \beta_W | \mathcal{X}_{k+1,i})$ is the linear transfer function (i.e., RAO) between wave elevation and the vessel motion of interest corresponding to $x_j(t)$, which depends on the state sigma point $\mathcal{X}_{k+1,i}$ and the location and quantity j. $S_{\zeta\zeta}(\omega, \beta_W | \mathcal{X}_{k+1,i}^\theta)$ is the single-sided wave spectrum, $S_{j,i}$ is the corresponding response spectrum, its standard deviation $\sigma_{j,i}$ is the predicted measurement for the measured quantity j at sigma point $\mathcal{X}_{k+1,i}$, N_ω is the number of discrete frequencies of the response spectrum, and $\Delta\omega_n$ is the frequency interval for ω_n. $\Delta\omega_n$ may be different for different discrete frequencies ω_n. For cases considering long-crested waves, 241 discrete frequencies were applied.

When a 2D wave or a short-crested wave is considered, Eq. (8) will consequently become:

$$S_{j,i}(\omega) = \sum_{\beta_W} |H_j(\omega, \beta_W | \mathcal{X}_{k+1,i})|^2 S_{\zeta\zeta}(\omega, \beta_W | \mathcal{X}_{k+1,i}^\theta) \Delta\beta_W \tag{9a}$$

$$\sigma_{j,i} = \sqrt{\sum_{n=1}^{N_\omega} S_{j,i}(\omega_n) \cdot \Delta\omega_n} \tag{9b}$$

where $\Delta\beta_W$ is the wave direction interval and $\Delta\beta_W = 2°$ was applied. Evenly distributed frequencies ($N_\omega = 400$) at each discrete direction between periods of 3 s and 40 s were applied in the sensitivity study for short-crested waves when calculating the predicted measurements $\sigma_{j,i}$.

The predicted measurement $Z_{k+1,i}$ based on the sigma point $\mathcal{X}_{k+1,i}$ for $j = 1, 2, \ldots, J$ can be written as

$$Z_{k+1,i} = \begin{bmatrix} \sigma_{1,i} \\ \sigma_{2,i} \\ \vdots \\ \sigma_{J,i} \end{bmatrix} \tag{10}$$

Accordingly, the measurement update step can be formulated as

$$\mathcal{Z}_{k+1} = \sum_{i=0}^{2N} w_i^m Z_{k+1,i} \tag{11a}$$

$$y_{k+1} = z_{k+1} - \mathcal{Z}_{k+1} \tag{11b}$$

$$P_{z_{k+1}} = \sum_{i=0}^{2N} w_i^c (Z_{k+1,i} - \mathcal{Z}_{k+1})(Z_{k+1,i} - \mathcal{Z}_{k+1})^\top + R_{k+1} \tag{11c}$$

$$P_{xz_{k+1}} = \sum_{i=0}^{2N} w_i^c (\mathcal{X}_{k+1,i} - \bar{x}_{k+1})(Z_{k+1,i} - \mathcal{Z}_{k+1})^\top \tag{11d}$$

$$K = P_{xz_{k+1}} P_{z_{k+1}}^{-1} \tag{11e}$$

$$x_{k+1} = \bar{x}_{k+1} + K y_{k+1} \tag{11f}$$

$$P_{k+1} = \bar{P}_{k+1} - K P_{z_{k+1}} K^\top \tag{11g}$$

where $\mathcal{Z}_{k+1} \in \mathbb{R}^J$ is the predicted measurement vector based on the sigma points $\mathcal{X}_{k+1}$, y_{k+1} is the residual between the predicted measurement $\mathcal{Z}_{k+1}$ and the acquired measurement z_{k+1}. R_{k+1} represents the measurement noise and the uncertainties of the measurement functions as shown in Eq. (8). R_{k+1} can be sensor and sea state dependent. $P_{z_{k+1}} \in \mathbb{R}^{J \times J}$ is the covariance matrix of the sigma points in measurement space, $P_{xz_{k+1}} \in \mathbb{R}^{N \times J}$ is the cross covariance of the state and the measurement. K is known as the Kalman gain which is used for updating the state and its covariance matrix. The updated state and its covariance for step $k + 1$ are denoted by x_{k+1} and P_{k+1} respectively.

Accordingly, a complete loop is described for recursively tuning of the uncertain vessel parameters and the sea state characteristics, and reducing their uncertainties.
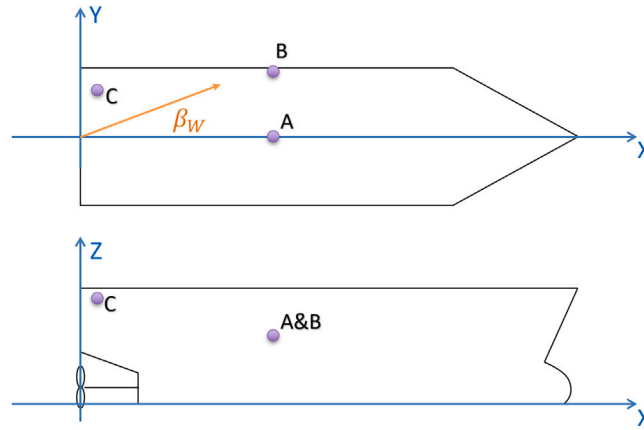
Fig. 2. The reference coordinate system and the locations of the virtual sensors measuring vessel motions.

Table 3
Description of sensor measurements.

Sensor ID	Location	Signal/measurements
Displacement_A	A	$\eta_3(t)$ at location A
Displacement_B	B	$\eta_3(t)$ at location B
Displacement_C	C	$\eta_3(t)$ at location C
Velocity_A	A	$\dot{\eta}_3(t)$ at location A
Velocity_B	B	$\dot{\eta}_3(t)$ at location B
Velocity_C	C	$\dot{\eta}_3(t)$ at location C
Acceleration_A	A	$\ddot{\eta}_3(t)$ at location A
Acceleration_B	B	$\ddot{\eta}_3(t)$ at location B
Acceleration_C	C	$\ddot{\eta}_3(t)$ at location C

$\eta_3(t)$: time series of heave displacement;
$\dot{\eta}_3(t)$: time series of heave velocity;
$\ddot{\eta}_3(t)$: time series of heave acceleration.

4. Basis of case studies

The algorithm is demonstrated by case studies based on a typical offshore supply vessel (OSV) where the wave information and vessel motion measurements are numerically simulated with addition of white noise. It is assumed that the wave-induced vessel motion in the wave frequency range can be well estimated by the linear transfer functions (i.e., RAOs) and the wave spectrum in the frequency domain, for moderate seas. The RAOs were generated by application of DNV GL advanced seakeeping analysis software Wasim [50].

4.1. Scope of the base case

Earlier research [2] suggests that multiple vessel motion sensors at different locations providing signals of displacements, velocities, and accelerations can help to identify the correct uncertain vessel parameters and tune towards their true values. Therefore, the case studies considered virtual sensors at three different locations onboard (i.e., locations A, B, and C) as illustrated in Fig. 2 and summarized in Table 3, measuring the corresponding heave displacements, velocities, and accelerations. The vessel coordinate system is also illustrated in Fig. 2. The origin is at the stern of the keel elevation. The positive X-axis points towards the bow, the positive Y-axis points towards the port, and the positive Z-axis points vertically upwards. The wave direction β_W, also shown in Fig. 2, follows the same coordinate system, in a positive going-to convention, where for example, $\beta_W = 180°$ corresponds to a head sea condition.

Zero vessel forward speed was considered for simplicity to avoid the 3-to -1 mapping problem for following seas [51]. However, the proposed algorithm and framework is so flexible that vessel forward speed can definitely be included in the vessel state ϕ. Earlier studies [2,25] show that the interesting vessel motions listed in Table 3 are sensitive to the linearized additional roll damping coefficient β_{44} and the longitudinal center of gravity XCG. In reality, application of a multi-peak wave spectrum consisting of both wind sea and swell components might be needed. However, single peak long-crested Pierson–Moskowitz (PM) wave spectra [42] as shown in Eq. (12) are assumed for simplification.

$$S_{\zeta\zeta}(\omega) = \frac{5}{16} H_s^2 \omega_p^4 \omega^{-5} \exp\left(-\frac{5}{4}\left(\frac{\omega}{\omega_p}\right)^{-4} \right) \tag{12}$$
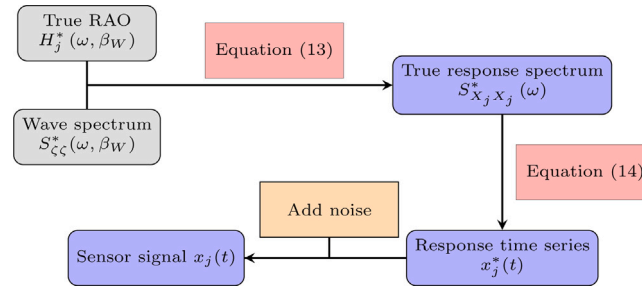
Fig. 3. Process of generating virtual sensor signal $x_j(t)$ for sensor j.

where ω_p is the sea state peak frequency. The error due to the uncertain wave spectral shape may be included in the measurement noise covariance matrix $\boldsymbol{R}$.

For demonstration purposes, the uncertain vessel parameters $\boldsymbol{\phi} = [\beta_{44}, XCG]^\top$ as the vessel state, and the uncertain sea state characteristics $\boldsymbol{\theta} = [H_s, T_p, \beta_W]^\top$ as the sea state, were considered for the base case study. The selected true vessel state is $\boldsymbol{\phi}^* = [\beta_{44}^*, XCG^*]^\top = [4\%, 61.4 \text{ m}]^\top$. Consequently, the true RAO for each virtual sensor can be determined, denoted by $H_j^*(\omega, \beta_W)$. Virtual sensor signals are numerically simulated, as illustrated in Fig. 3. Based on the true vessel motion RAO $H_j^*(\omega, \beta_W)$ corresponding to the sensor measurement $x_j(t)$ and the true wave spectrum $S_{\zeta\zeta}^*(\omega, \beta_W)$, the corresponding true vessel motion spectrum $S_{X_jX_j}^*(\omega)$ can be calculated by Eq. (13) assuming long-crested wave conditions as the base case.

$$S_{X_jX_j}^*(\omega) = |H_j^*(\omega, \beta_W)|^2 S_{\zeta\zeta}^*(\omega, \beta_W) \tag{13}$$

Then a vessel motion realization (i.e., $x_j^*(t)$) can be generated by:

$$x_j^*(t) = \sum_{n=1}^{N_\omega} C_n(\omega_n)\cos(\omega_n t + \varphi_n + \psi_{j,n}) \tag{14a}$$

$$C_n(\omega_n) = \sqrt{2 S_{X_jX_j}^*(\omega_n) \cdot \Delta\omega_n} \tag{14b}$$

where ω_n is the discrete frequency, $\Delta\omega_n$ is the interval of ω_n, and N_ω is the total number of discrete frequencies for $S_{X_jX_j}^*(\omega_n)$. $\varphi_n \in [0, 2\pi)$ is a continuous and uniformly distributed random phase angle for the wave component at ω_n, $\psi_{j,n} \in [-\pi, \pi)$ is the phase angle between the wave elevation and the vessel response at ω_n corresponding to the signal $x_j(t)$. For example, the complex-valued linear transfer function $H_j(\omega, \beta_W)$ equals to $|H_j(\omega_n, \beta_W)| \exp(1i \times \psi_{j,n})$. $S_{X_jX_j}^*(\omega_n)$ for periods between 3 s and 40 s was considered. In order to sufficiently capture the spectral information at the periods of main interest and reduce the numerical integration error, the period intervals (i.e., ΔT_n) for the discrete periods from 5 s to 25 s were set to 0.125 s. For periods from 3 s to 5 s and from 25 s to 26 s, ΔT_n was set to 0.25 s; and for periods from 26 s to 40 s, ΔT_n is 0.5 s. Consequently, the frequency intervals $\Delta\omega_n$ applied in Eq. (14) were unevenly distributed, thus avoiding time record repetition.

Finally, the virtual signal $x_j(t)$ was generated by adding noise to each time step of $x_j^*(t)$. Independent Gaussian distributed white noise was assumed with specified signal-to-noise ratio (SNR):

$$SNR = \frac{\sigma_{X_j}^2}{\sigma_N^2} \tag{15}$$

where $\sigma_{X_j}^2$ is the variance of the true response spectrum and σ_N^2 is the noise variance.

Each case study considered 20 randomly generated sea states. Each sea state was assumed to last for 30 min. No transition between sea states was considered, thus assuming that each sea state is independent from the others. The values of the key parameters for the base case study are summarized in Table 4 with respect to case simulations and in Table 5 with respect to UKF modeling. The initial state is also summarized in Table 5.

Please note that ε_{H_s}, ε_{T_p}, and ε_{β_W} are the errors from the acquired wave information which are random and Gaussian distributed, i.e.,

$$\varepsilon_{H_s} = \sigma_{H_s} \cdot \text{rand}[\mathcal{N}(0,1)] \sim \mathcal{N}(0, \sigma_{H_s}^2) \tag{16a}$$

$$\varepsilon_{T_p} = \sigma_{T_p} \cdot \text{rand}[\mathcal{N}(0,1)] \sim \mathcal{N}(0, \sigma_{T_p}^2) \tag{16b}$$

$$\varepsilon_{\beta_W} = \sigma_{\beta_W} \cdot \text{rand}[\mathcal{N}(0,1)] \sim \mathcal{N}(0, \sigma_{\beta_W}^2) \tag{16c}$$

where σ_{H_s}, σ_{T_p}, and σ_{β_W} are the standard deviations of the acquired wave information (i.e., H_s, T_p, and β_W) as indicated in Table 2, representing their uncertainties. $\text{rand}[\mathcal{N}(0,1)]$ means a randomly selected value from an unit normal distribution i.e., $\mathcal{N}(0,1)$. A lowpass filter based on fast Fourier transform (FFT) was applied for each sensor signal to remove the signal noises as much as

Table 4
Applied parameters in the base case simulation.

Parameter	Value
$H_s^{*\,\text{a}}$	Uniformly distributed in [1.0, 4.0] m
$T_p^{*\,\text{a}}$	Uniformly distributed in [5.0, 20.0] s
$\beta_W^{*\,\text{a}}$	Uniformly distributed in [0.0°, 360.0°]
σ_{H_s}	$10\% H_s^*$ m
σ_{T_p}	0.5 s
σ_{β_W}	5°
$\overline{H}_s^{\,\text{b}}$	$H_s^* + \varepsilon_{H_s}$
$\overline{T}_p^{\,\text{b}}$	$T_p^* + \varepsilon_{T_p}$
$\overline{\beta}_W^{\,\text{b}}$	$\beta_W^* + \varepsilon_{\beta_W}$
Initial seed τ	44
Sea state duration	1800 s
Number of sea states	20
SNR	50
f_{lp}	0.2 Hz

[a]Superscript $*$ means the true value of the corresponding parameters. The acquired wave information $(\overline{H}_s,\ \overline{T}_p,\ \overline{\beta}_W)$ is subject to errors (i.e., ε_{H_s}, ε_{T_p}, and ε_{β_W}).

[b]The overlines over the parameters means that they are the simulated acquired values which can be different from the true values.

Table 5
Applied parameters in the base case related to UKF modeling.

Parameter	Value
State $\boldsymbol{x}$	$\boldsymbol{x} = [\beta_{44}, XCG, H_s, T_p, \beta_W]^\top$
Initial $\boldsymbol{\phi}_0$	$\boldsymbol{\phi}_0 = [\beta_{44}, XCG]^\top = [7\%, 59.4 \text{ m}]^\top$
Initial $\boldsymbol{P}_{\phi_0}$	$\boldsymbol{P}_{\phi_0} = \text{diag}(0.035^2, 4.0^2)$
$\boldsymbol{R}$	$\boldsymbol{R} = 2\% \cdot \text{diag}(\hat{\sigma}_1^2, \ldots, \hat{\sigma}_j^2)$
$\boldsymbol{Q}$	$\boldsymbol{Q} = \text{diag}(0.005^2, 0.1, 0.05^2, 0.01, 0.25)$
α	0.01
β	2
κ	-2

possible. A SNR of 50 was considered. Sensitivity studies with respect to the SNR (varied from 30 to 200) showed very stable tuning performance due to the application of a lowpass filter to remove the high-frequency noises as accurately as possible. Ideally, the cutoff frequency f_{lp} should be sea state and vessel dependent. For simplicity, a constant cutoff frequency $f_{lp} = 0.2$ Hz was applied. Please note that the initial seed τ uniquely determines the true sea states, the normalized random values of rand$[\mathcal{N}(0,1)]$ (and consequently the acquired wave information with the same parameter uncertainties), and the random phase angles φ_n for the time series from the deterministic discrete frequencies. Consequently, τ uniquely determines the simulated sea states and the virtual sensor signals in the coded program for the long-crested wave conditions. The randomly generated values of rand$[\mathcal{N}(0,1)]$ for ε_{H_s}, ε_{T_p}, and ε_{β_W} are independent.

The measurement uncertainty covariance matrix $\boldsymbol{R}$ is a diagonal matrix. For each sensor j, the measurement variance was set to be 2% of the variance of the filtered sensor signal $\hat{\sigma}_j^2$. Small values were used for the process uncertainty covariance matrix $\boldsymbol{Q}$, which represents how well the propagation model can describe the process. For the numerical simulation, a stationary condition was fulfilled so that the proposed propagation model can very well represent the simulated conditions. However, slow-varying characteristics may be commonly seen in reality for the vessel and wave conditions. Therefore, the values of the $\boldsymbol{Q}$ matrix should be increased to reflect this effect. Initial sensitivity studies of key parameters in the UKF model indicate that a smaller α generally leads to better performance. UKF with smaller α selects the sigma points closer to each other so that the local effects are more displayed, while UKF with larger α tends to focus more on the global system behavior. Therefore, a smaller value of α is preferred for highly nonlinear problems. On the other hand, a small α easily leads to a negative weight factor w_0^c for large dimensional problems, and thus cannot guarantee a positive semi-definite state covariance matrix $\boldsymbol{P}$. Such a challenge was not noted during the performance of the simulations and therefore, no modification to the proposed algorithm was made.

Initial studies also indicated that it is beneficial to use a slightly larger initial covariance matrix for the vessel state, $\boldsymbol{P}_{\phi_0}$. A larger initial $\boldsymbol{P}_{\phi_0}$ will accelerate the vessel state convergent towards their true values, and $\boldsymbol{P}_{\phi}$ will approach its convergent value which is independent from its initial value.

Table 6
Range of vessel model parameters in the RAO database.

Parameters	Variation range	Number of values
β_{44}	[2%, 14%]	7
XCG	[55.4 m, 63.4 m]	5

Table 7
Applied parameters in the base case related to UKF modeling.

Parameter	Value
n_s^*	Uniformly distributed in [2.0, 5.0]
$\bar{n}_s$	3.5
σ_{n_s}	1.0
State x	$x = [\beta_{44}, XCG, H_s, T_p, \beta_W, n_s]^\top$
Q	$Q = \text{diag}(0.005^2, 0.1, 0.05^2, 0.01, 0.25, 0.09)$
κ	−3

4.2. Measurement functions

The measurement function as shown in Eqs. (8) and (10) varies with the calculated sigma points. Therefore, seakeeping analysis is preferably performed for each determined sigma point as illustrated in Fig. 1. However, for simplicity, a RAO database with limited amount of combinations of uncertain vessel parameters inherited from earlier research work [25] was used. The available discrete values of β_{44} and XCG in the RAO database are summarized in Table 6. The measurement estimation (i.e., the standard deviations of the interesting vessel motions $\sigma_j(\beta_{44}, XCG)$) can be approximated by linear interpolation of neighboring values $\sigma_j(\beta'_{44}, XCG')$, $\sigma_j(\beta''_{44}, XCG')$, $\sigma_j(\beta'_{44}, XCG'')$, $\sigma_j(\beta''_{44}, XCG'')$ calculated based on the available RAOs in the RAO database, where β'_{44}, XCG', β''_{44}, XCG'' are the available values in the RAO database and $\beta'_{44} < \beta_{44} < \beta''_{44}$, $XCG' < XCG < XCG''$.

The uncertainties caused by applying linear RAOs as the system model may consist of model bias and model scatter. The model bias is the average model error compared with the actual system, whereas the random component with respect to the model bias refers to the model scatter [52]. The model bias may be introduced by simplifications and assumptions made in the seakeeping software and the numerical model. However, zero model bias was assumed for the measurement function. The model scatter is accounted for by means of the measurement uncertainty covariance matrix R.

4.3. Short-crested waves

Long-crested waves barely exist in the real world. Therefore, it is worth demonstrating, as a sensitivity case study, how the short-crested waves can be considered in the proposed tuning framework. The short-crested wave condition may be approximated by multiplying the uni-directional PM wave spectrum with a directional spreading function $D(\beta_W)$ [42]:

$$S_{\zeta\zeta}(\omega, \beta_W) \approx S_{\zeta\zeta}(\omega)D(\beta_W) \tag{17a}$$

$$D(\beta_W) = \frac{\Gamma(1 + n_s/2)}{\sqrt{\pi}\,\Gamma(1/2 + n_s/2)} \cos^{n_s}(\beta_W - \beta_{Wp}) \tag{17b}$$

where Γ is the Gamma function, β_{Wp} is the prevailing wave direction and $|\beta_W - \beta_{Wp}| \leq \frac{\pi}{2}$. n_s is the spreading parameter, $2 \leq n_s \leq 4$ for wind sea, and $n_s > 7$ for swells [42]. Consequently, the spreading parameter n_s should therefore be included in the sea state vector θ. For the sensitivity study on short-crested waves, the applied key parameters that are different from the base case are summarized in Table 7. In reality, the acquired wave information may not contain the spreading information, e.g., in terms of n_s value. Therefore, the sensitivity study assumed that the estimation of n_s was not acquired from wave measurements, hindcast, or forecast. For each new sea state, n_s is set to be 3.5, with a variance of 1.0.

When short-crested waves are considered, Eqs. (13) and (14) are substituted by:

$$x_j^*(t) = \sum_{u=1}^{N_{\beta_W}} \sum_{v=1}^{N_\omega} C_{u,v} \cos(\omega_{u,v}t + \varphi_{u,v} + \psi_{j,u,v}) \tag{18a}$$

$$C_{u,v} = \sqrt{2S_{X_jX_j}^*(\omega_{u,v}, \beta_{W_u})\Delta\omega_{u,v}\Delta\beta_W} \tag{18b}$$

$$S_{X_jX_j}^*(\omega_{u,v}, \beta_{W_u}) = |H_j^*(\omega_{u,v}, \beta_{W_u})|^2 S_{\zeta\zeta}(\omega_{u,v}, \beta_{W_u}) \tag{18c}$$

where N_ω is the number of discrete frequencies $\omega_{u,v}$ for each wave direction β_{W_u}. The subscript of $\omega_{u,v}$ indicates that the values of discrete frequencies also depend on the wave direction. For each β_{W_u} in the sensitivity study of short-crested wave conditions, 800 discrete frequencies were randomly generated, assuming that frequencies are uniformly distributed between 0.157 rad/s and 2.094 rad/s (i.e., periods between 3 s and 40 s), in order to avoid non-ergodic wave realizations [53]. Compared with long-crested wave conditions, much more discrete frequencies were generated for each direction in order to assure a sufficiently small frequency

interval at the frequency range of main interest. Consequently, $\Delta\omega_{u,v}$ differs for each $\omega_{u,v}$. Constant $\Delta\beta_W$ of 2° was considered. $\varphi_{u,v} \in [0, 2\pi)$ is the random phase angle for wave component at $(\omega_{u,v}, \beta_{W_u})$, $\psi_{j,u,v} \in [-\pi, \pi)$ is the phase angle for the linear transfer function $H_j^*(\omega_{u,v}, \beta_{W_u})$. The power spectral density of the short-crested waves $S_{\zeta\zeta}(\omega_{u,v}, \beta_{W_u})$ can be calculated according to Eq. (17).

5. Results

New parameters $\%\Delta\sigma_{H_s}^2$, $\%\Delta\sigma_{T_p}^2$, and $\%\Delta\sigma_{\beta_W}^2$ are defined in order to present the relative reduction of the variance in percentage for the corresponding sea state characteristics.

$$\%\Delta\sigma_{H_s}^2 = \frac{\sigma_{H_s}^2 - \hat{\sigma}_{H_s}^2}{\sigma_{H_s}^2} \times 100\% \tag{19a}$$

$$\%\Delta\sigma_{T_p}^2 = \frac{\sigma_{T_p}^2 - \hat{\sigma}_{T_p}^2}{\sigma_{T_p}^2} \times 100\% \tag{19b}$$

$$\%\Delta\sigma_{\beta_W}^2 = \frac{\sigma_{\beta_W}^2 - \hat{\sigma}_{\beta_W}^2}{\sigma_{\beta_W}^2} \times 100\% \tag{19c}$$

where $\sigma_{H_s}^2$, $\sigma_{T_p}^2$, and $\sigma_{\beta_W}^2$ represents the variance of the acquired sea state characteristics, while $\hat{\sigma}_{H_s}^2$, $\hat{\sigma}_{T_p}^2$, and $\hat{\sigma}_{\beta_W}^2$ indicate their tuned values after measurement update.

$\Delta\overline{H}_s$, $\Delta\overline{T}_p$, and $\Delta\overline{\beta}_W$ are also defined to represent the difference between the true and the acquired wave information, while $\Delta\hat{H}_s$, $\Delta\hat{T}_p$, and $\Delta\hat{\beta}_W$ are defined to represent the difference between the true and the tuned values of the wave parameters after measurement update stage, i.e.,

$$\Delta\overline{H}_s = \varepsilon_{H_s} = H_s^* - \overline{H}_s \tag{20a}$$

$$\Delta\overline{T}_p = \varepsilon_{T_p} = T_p^* - \overline{T}_p \tag{20b}$$

$$\Delta\overline{\beta}_W = \varepsilon_{\beta_W} = \beta_W^* - \overline{\beta}_W \tag{20c}$$

and

$$\Delta\hat{H}_s = H_s^* - \hat{H}_s \tag{21a}$$

$$\Delta\hat{T}_p = T_p^* - \hat{T}_p \tag{21b}$$

$$\Delta\hat{\beta}_W = \beta_W^* - \hat{\beta}_W \tag{21c}$$

5.1. Base case

The randomly generated sea states according to Table 4 for the base case are summarized in Table 8 and the tuning results are summarized in Table 9. k indicates the sea state number. A superscript $*$ indicates the true value of the parameter, while an overline over the parameter means the corresponding acquired (prior) information. A hat ˆ over the parameter indicates its value after the measurement update step for the corresponding sea state k.

Fig. 4 shows the standard deviations of the filtered sensor signals (blue points) and the corresponding estimated standard deviations of the vessel responses (i.e., the "predicted measurements") by transferring the system states from the state space to the measurement space based on the unscented transformation described in Section 3.4. The difference between the acquired and the predicted measurement is the residual **y** defined in Eq. (11b). Fig. 5 illustrates how the uncertain vessel parameters β_{44} and XCG vary through the simulation. The dotted green lines are the true values. The black lines are the predicted values of the uncertain parameters after the system propagation described in Section 3.3, while the filled gray areas indicate the corresponding 95% confidence interval for the parameters, i.e., $\pm 2\sigma$ where σ is the variable standard deviation. The red lines are the updated values after the measurement update step described in Section 3.4, and the filled red areas indicate the corresponding 95% confidence interval. Fig. 5 shows a successful tuning of β_{44} and XCG and reduction of their uncertainties.

While the proposed algorithm managed to tune the uncertain vessel parameters, knowledge about the sea state characteristics were also improved simultaneously, as shown in Figs. 6 to 8. Generally, the tuning algorithm helped to reduce the overall errors and variance from the acquired wave information. For example, the largest error of the acquired H_s (i.e., $\Delta\overline{H}_s$) happened at $k = 9$. The tuning algorithm managed to reduce such errors from 0.5 m to 0.2 m. Furthermore, the information variance on H_s was reduced by 58%. Even though increased errors after tuning were observed for some sea states (e.g., $k = 6$, 13, 18), it only happened when the error from the acquired information was already relatively small. In addition, such increased errors did not prevent the system from significantly reducing the uncertainty (variance). In comparison, error reduction with respect to T_p and β_W may not be that dramatic, because the influence of T_p and β_W on the vessel motions is not as monotonous and simple as that of H_s. Please note that error reduction is different from uncertainty reduction. There is a significant possibility that for a certain parameter (e.g., H_s) the error increases while its variance reduces.
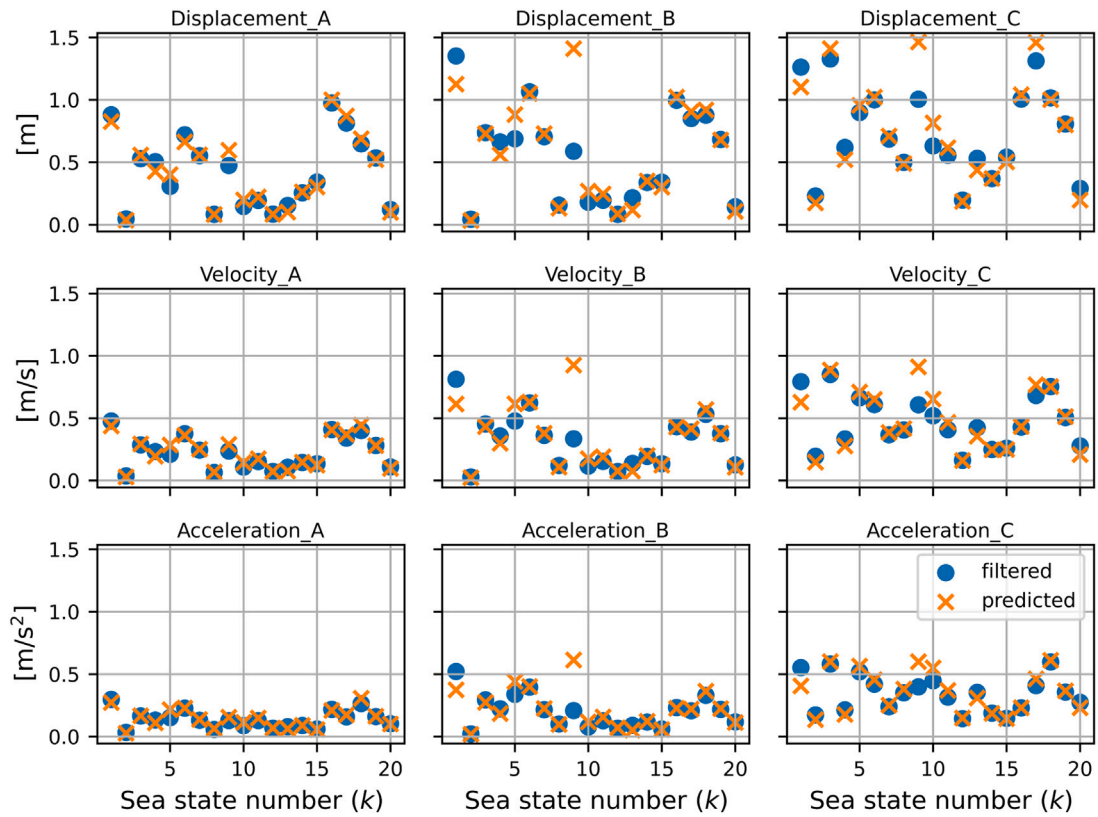
Fig. 4. The acquired (after signal filtering) and predicted measurements for the base case from the 9 virtual sensors described in Table 3 for the 20 sea states, base case $\tau = 44$.
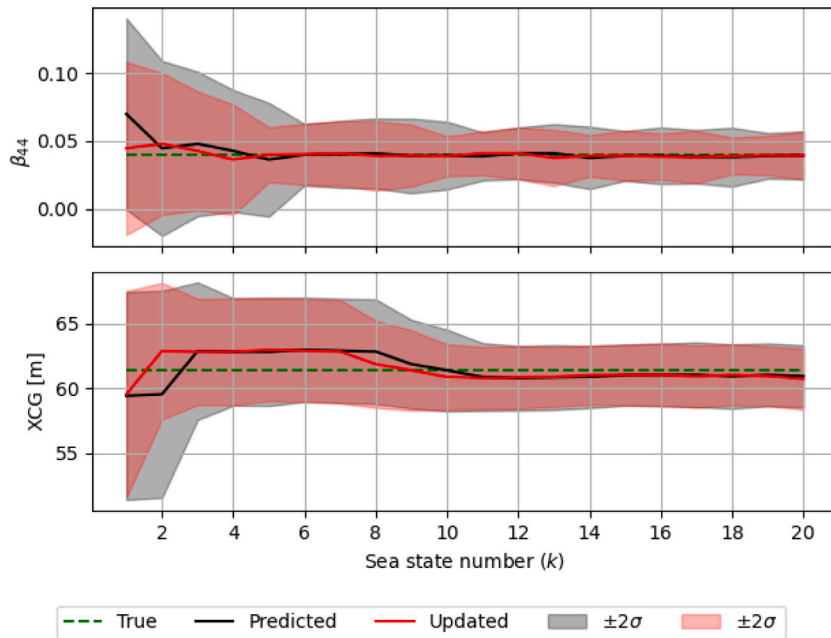

Fig. 5. The results of tuning β_{44} and XCG for the base case $\tau = 44$. (For interpretation of the references to color in this figure legend, the reader is referred to the web version of this article.)

Table 8
The true and the acquired sea state characteristics for the base case.

k	H_s^*	T_p^*	β_W^*	$\overline{H}_s$	$\overline{T}_p$	$\overline{\beta}_W$
1	3.5	14.6	256.0	3.3	15.3	257.9
2	1.3	7.1	26.1	1.1	7.1	22.1
3	3.2	11.9	317.7	3.5	12.2	323.5
4	2.1	18.1	261.4	1.7	18.0	261.5
5	2.1	8.9	300.0	2.2	9.1	290.5
6	2.8	15.0	255.7	2.8	14.1	251.4
7	2.2	17.9	251.1	2.3	18.0	250.8
8	2.2	7.2	334.8	2.4	6.9	341.0
9	2.5	13.4	317.4	3.0	14.1	314.7
10	3.1	7.4	34.2	3.6	7.8	32.5
11	3.9	7.6	164.3	4.3	7.5	156.6
12	2.4	6.6	177.4	2.7	6.2	183.5
13	2.3	8.0	39.2	2.3	7.6	27.9
14	1.3	11.8	55.3	1.4	12.1	56.4
15	1.7	16.9	354.3	1.6	16.6	354.1
16	3.9	19.9	97.8	4.0	20.7	99.2
17	3.8	17.1	323.0	4.3	16.5	326.0
18	3.6	10.7	59.1	3.6	10.3	64.3
19	2.9	12.7	47.6	2.9	12.2	47.7
20	1.6	5.9	114.2	1.5	5.2	105.5

Table 9
Tuning results for base case.

k	$\hat{H}_s$	$\hat{T}_p$	$\hat{\beta}_W$	$\%\Delta\sigma^2_{H_s}$	$\%\Delta\sigma^2_{T_p}$	$\%\Delta\sigma^2_{\beta_W}$	$\hat{\beta}_{44}$	$\widehat{XCG}$	$\hat{\sigma}^2_{\beta_{44}}$	$\hat{\sigma}^2_{XCG}$
1	3.7	15.1	258.0	67%	7%	16%	0.045	59.53	1.02E−03	15.87
2	1.2	7.3	22.6	18%	65%	8%	0.048	62.86	6.88E−04	6.94
3	3.4	12.1	322.4	51%	18%	37%	0.043	62.80	4.84E−04	4.21
4	2.0	17.9	261.8	69%	5%	10%	0.036	62.80	4.15E−04	4.25
5	2.0	9.0	297.1	54%	20%	67%	0.040	62.97	1.03E−04	3.94
6	2.7	14.2	252.4	57%	8%	35%	0.040	62.89	1.28E−04	3.95
7	2.2	18.1	250.5	67%	10%	27%	0.041	62.82	1.42E−04	3.98
8	2.3	7.1	338.2	31%	59%	43%	0.039	61.85	1.64E−04	2.83
9	2.7	14.0	317.8	58%	18%	55%	0.039	61.37	1.31E−04	2.38
10	3.4	7.5	29.8	34%	64%	33%	0.039	60.86	5.41E−05	1.60
11	4.1	7.3	159.4	41%	62%	31%	0.041	60.77	6.61E−05	1.45
12	2.7	6.2	182.2	20%	76%	22%	0.041	60.82	9.11E−05	1.46
13	2.5	8.4	30.7	40%	68%	8%	0.038	60.86	1.08E−04	1.33
14	1.3	12.0	55.6	47%	15%	34%	0.039	61.01	5.94E−05	1.30
15	1.6	16.6	354.1	72%	10%	2%	0.039	61.02	8.44E−05	1.35
16	4.0	20.6	98.8	72%	6%	23%	0.039	61.03	7.28E−05	1.45
17	3.9	16.6	326.6	69%	14%	42%	0.038	60.90	9.29E−05	1.44
18	3.6	10.3	61.5	59%	22%	58%	0.039	61.02	4.59E−05	1.37
19	2.9	12.3	47.7	61%	16%	40%	0.039	60.92	5.29E−05	1.33
20	1.6	5.5	109.1	11%	74%	39%	0.039	60.70	7.78E−05	1.39

The base case took approximately 120 s to run on the available laptop (CPU Intel(R) TM i7-8650U @ 1.90 GHz, 32 GB memory), from generating signals for the first sea state to updating the state vector for the last sea state, meaning that tuning of 5 parameters for each sea state approximately needs 6 s (including virtual sensor signal generation time). As an indicative comparison, Han et al. [25] reported that tuning of 4 parameters for one sea state approximately needs 90 s, running on the same laptop. Extraordinary improvement of computational efficiency is therefore demonstrated.

5.2. Seed variation

Simulations with different initial seed (τ) values other than 44 were performed. Generally, very stable tuning of β_{44} has been observed across all initial seeds. However, a convergent tuning result for XCG may not be observed after 20 sea states for some initial seed values, e.g., as shown in Fig. 9 with a value of $\tau = 16$. Earlier vessel parametric sensitivity studies [2] documented that the sensitivity of XCG on the vessel response varies with wave headings and wave periods, and the influence of XCG to the vessel response is generally less than the additional roll damping coefficient β_{44}. Therefore, a less accurately tuned XCG can be rational.

In general, tuning performance is very stable. Divergent tuning results have not been observed. However, less stable tuning may occur when insignificant vessel response is expected, e.g., at sea states with very small wave spectral peak periods. Consequently, the tuning can be very sensitive to the quality of signal filtering.
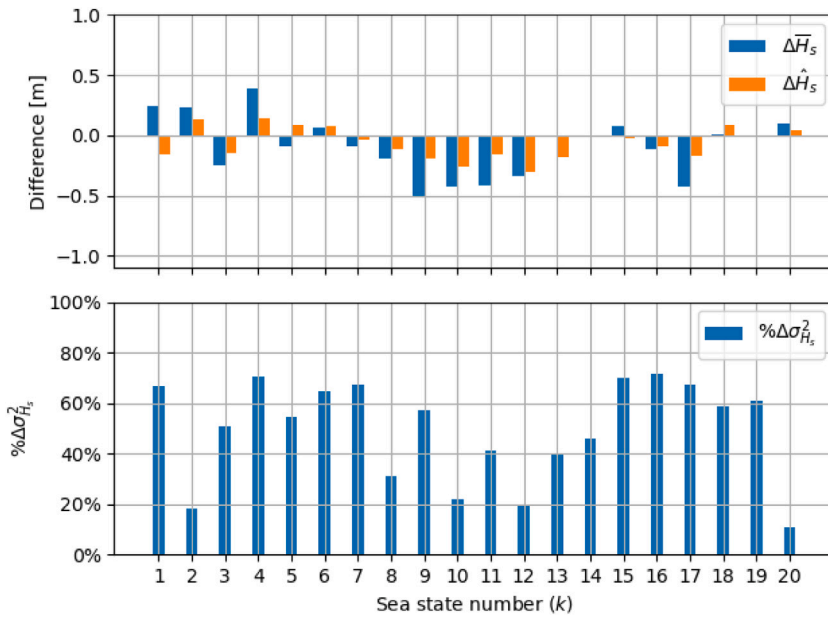
Fig. 6. Illustration of the errors before and after the tuning, and the variance reduction after tuning of H_s, for the base case $\tau = 44$.
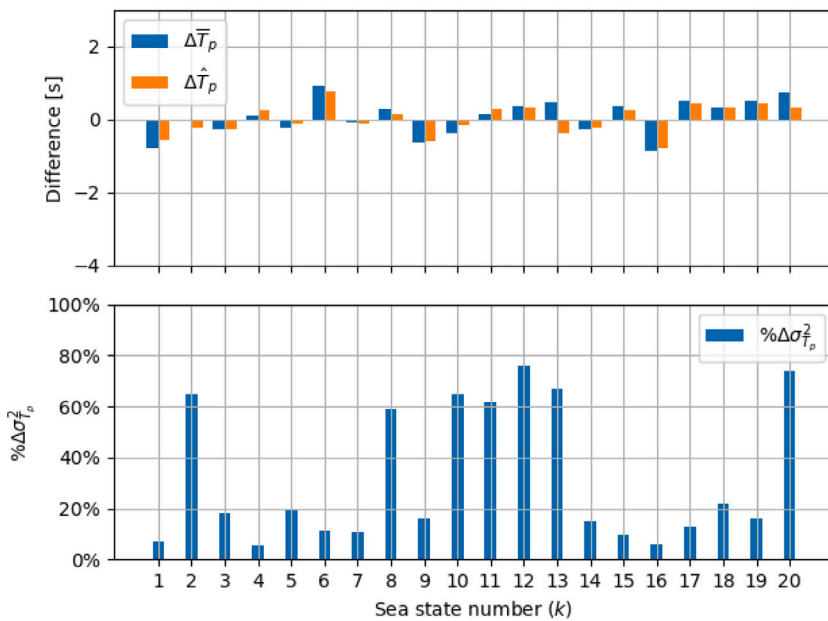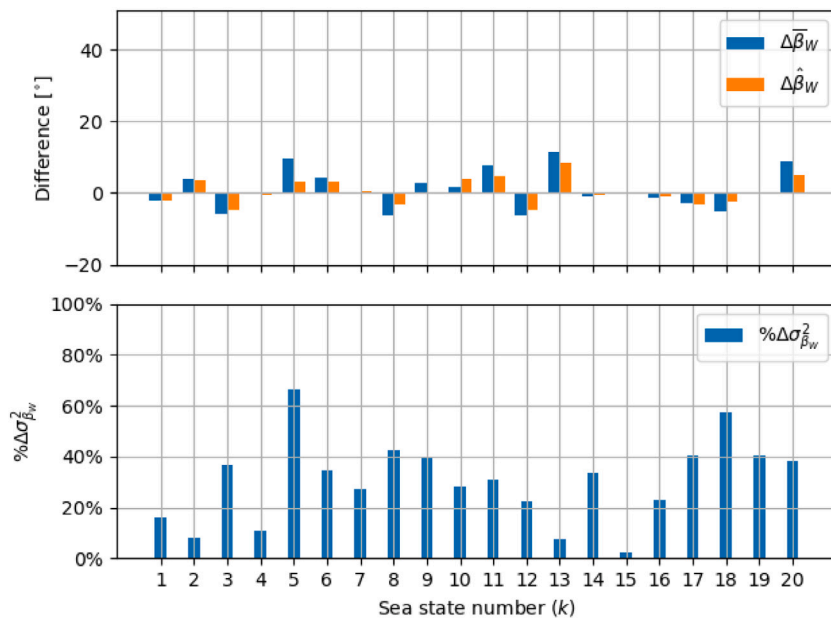

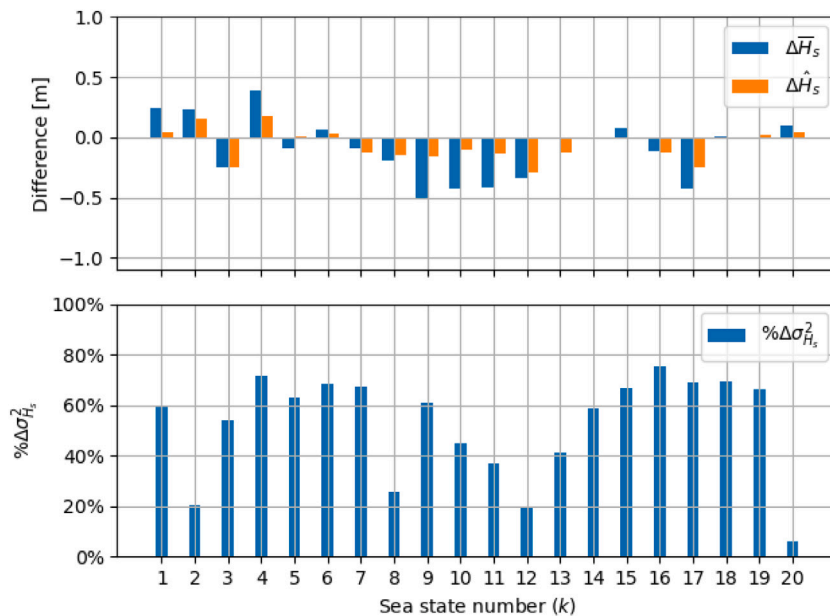**Fig. 7.** Illustration of the errors before and after the tuning, and the variance reduction after tuning of T_p, for the base case $\tau = 44$.

5.3. Short-crested waves

As described in Section 4.3, a sensitivity case study was performed, considering short-crested wave conditions. The applied parameters that are different from Tables 4 and 5 are summarized in Table 7.

As shown in Fig. 10, tuning of uncertain vessel parameters was slightly influenced due to the introduced additional uncertainty from the wave spreading parameter n_s. The tuning of H_s and T_p (Figs. 11 and 12) are much less influenced by the introduced wave spreading and the uncertain n_s. Including uncertainty of wave spreading n_s can significantly influence the tuning of wave direction β_W, in terms of both the tuned expected value and the variance reduction. Comparing between Figs. 13 and 8, significantly reduced

Fig. 8. Illustration of the errors before and after the tuning, and the variance reduction after tuning of β_W, for the base case $\tau = 44$.
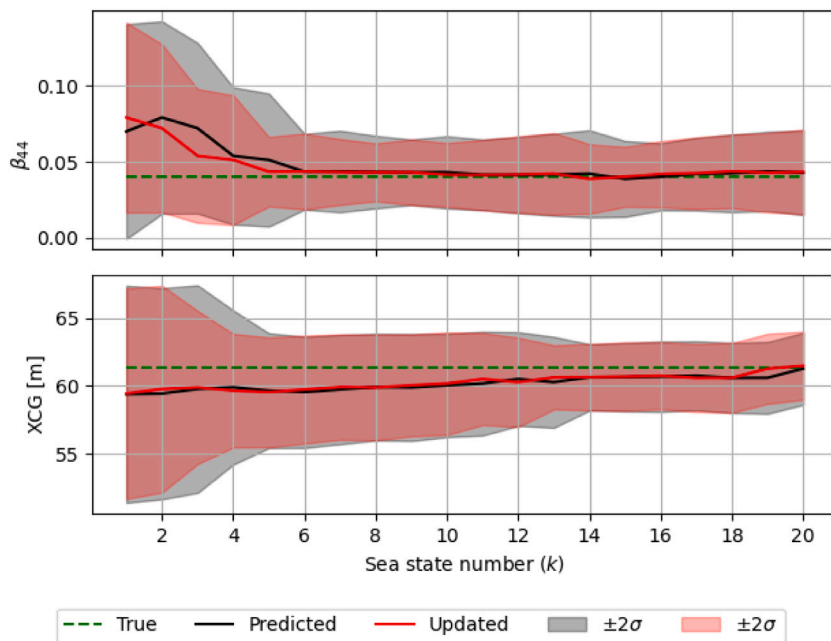
Fig. 9. The results of tuning β_{44} and XCG for the case with $\tau = 16$.

$\%\Delta\sigma^2_{\beta_W}$ are generally observed, indicating less confidence improvement of the prevailing wave direction when considering short-crested waves with the uncertain spreading parameter. In addition, information on n_s itself was not significantly improved as shown in Fig. 14. Negative $\%\Delta\sigma^2_{n_s}$ indicates the increased uncertainty on spreading parameter after tuning.

5.4. Sensitivity of wave information uncertainty

Uncertainties of the vessel state and the sea state are interacting in the proposed algorithm. An increasingly confident vessel seakeeping model can help improving the wave information, while more accurate wave information will help reducing the
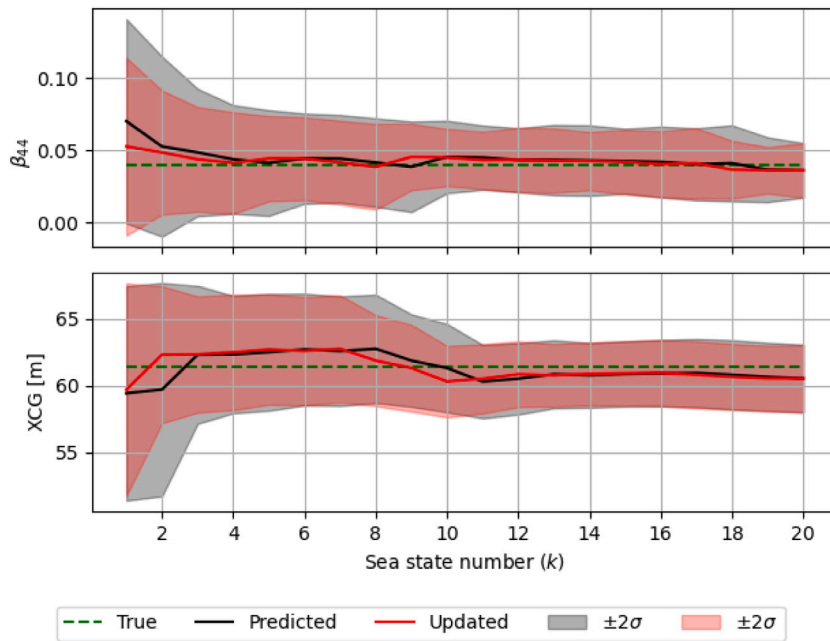
Fig. 10. The results of tuning β_{44} and XCG for the sensitivity study with respect to short-crested waves with $\tau = 44$.
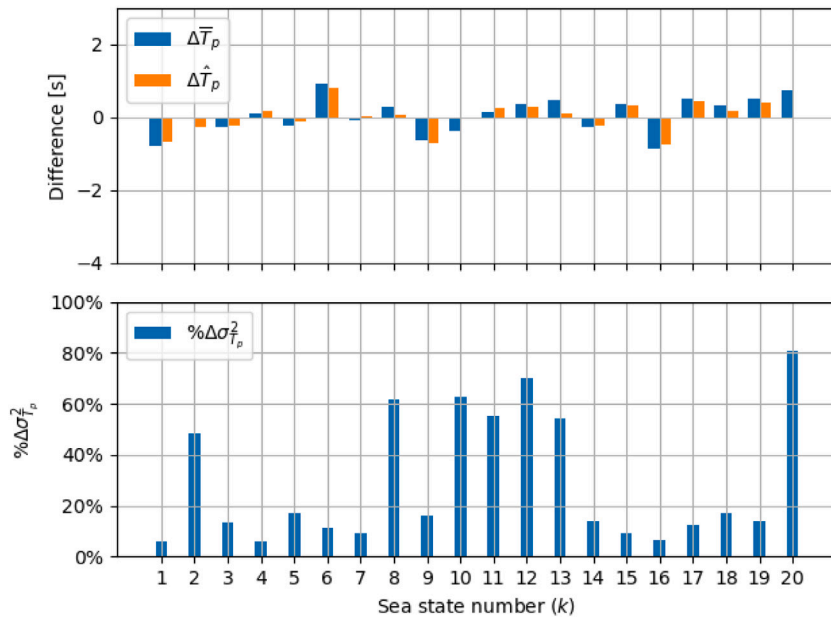

Fig. 11. Illustration of the errors before and after the tuning, and the variance reduction after tuning of H_s, for the sensitivity study with respect to short-crested waves with $\tau = 44$.

uncertainties of the vessel state. The base case assumed that the wave information can be acquired from measurements or hindcast, with a reasonably low uncertainty. However, such wave information may be delayed for several hours or up to some days. Therefore, it is interesting to test the algorithmic performance if the acquired wave information is subject to larger uncertainties when such wave measurements or hindcast data are not available. The alternative wave information source may come from forecast, visual observation, etc. Compared with the uncertainties of the WAM model in Table 1, much larger uncertainty of wave information was therefore considered in the sensitivity study, as shown in Table 10.

The same initial seed as for the base case was applied. Therefore, the same true sea states as shown in Table 8 were applied. The acquired sea states were consequently different from the base case, but the errors from the true sea states were proportional to

Fig. 12. Illustration of the errors before and after the tuning, and the variance reduction after tuning of T_p, for the sensitivity study with respect to short-crested waves with $\tau = 44$.
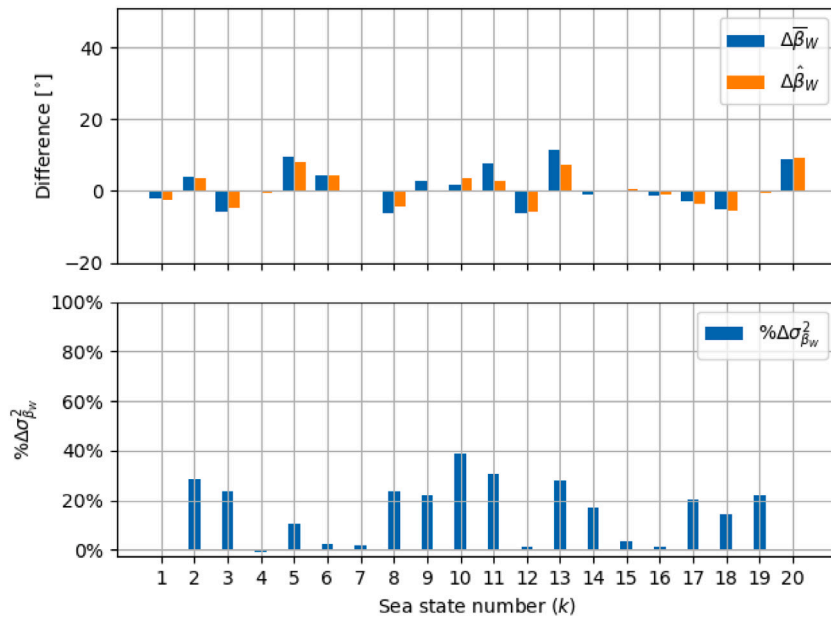
Fig. 13. Illustration of the errors before and after the tuning, and the variance reduction after tuning of β_W, for the sensitivity study with respect to short-crested waves with $\tau = 44$.

Table 10
Applied uncertainties of sea state characteristics in the sensitivity study with respect to wave information uncertainty.

Parameter	Standard deviation
σ_{H_s}	$20\% H_s^*$ m
σ_{T_p}	$10\% T_p^*$ s
σ_{β_W}	$15°$
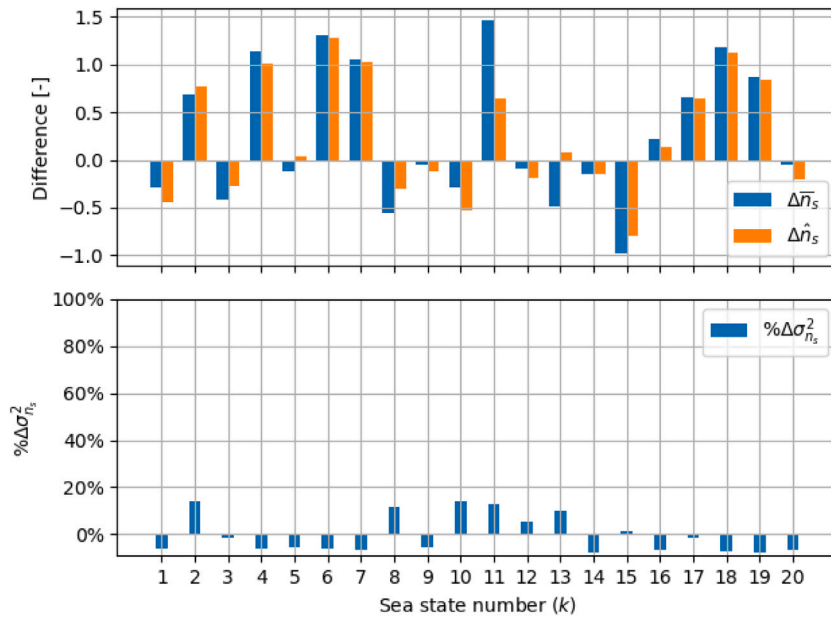
Fig. 14. Illustration of the errors before and after the tuning, and the variance reduction after tuning of n_s, for the sensitivity study with respect to short-crested waves with $\tau = 44$.

the corresponding errors in the base case. For example, the ratio of ε_{H_s} values between the base case and this sensitivity study was equal to the ratio of σ_{H_s} values between the base case and this sensitivity study.

Figs. 15 to 18 illustrate the tuning results of the vessel parameters and sea state characteristics based on larger wave information uncertainty. Fig. 15 shows a successful tuning of β_{44}. Whereas, convergent but slightly deviated tuning of XCG was observed when considering larger wave uncertainties. Compared with Fig. 5, the convergent XCG variance is larger when wave information is subject to larger variance, as shown in Fig. 15. Compared with the base case (e.g., at $k = 2$), the tuning of vessel state becomes smoother because of a relatively small Kalman gain in this sensitivity case. This means that the tuning algorithm rationally identifies larger uncertainty in the predicted measurements due to the specified larger wave information uncertainty. Consequently, the system reasonably focused more on improving the accuracy of the acquired wave information, as shown in Figs. 16 to 18. Significantly improved H_s, T_p, and β_W were observed compared with the base case. Much larger %$\Delta\sigma^2_{H_s}$, %$\Delta\sigma^2_{T_p}$, and %$\Delta\sigma^2_{\beta_W}$ are shown in Figs. 16 to 18 compared with Figs. 6 to 8 in the base case.

6. Conclusions and future work

A computationally cheap and efficient algorithm for tuning of uncertain vessel seakeeping model parameters and important characteristics of wave information has been proposed. The algorithm is founded on the so-called unscented transformation and the corresponding scaled unscented Kalman filter, which can efficiently handle large dimensional problems and take the system nonlinearity into account. Its performance has been demonstrated by numerically simulated case studies based on an OSV. The benefit of including sea state characteristics in the system state vector is that the uncertainties of wave information can also be reduced through the process. The proposed method continuously improves the simultaneous knowledge about the vessel state and the sea state information based on the onboard vessel motion measurements and the acquired wave data. Reasonable tuning results can still be achieved even with higher wave information uncertainties as described in Section 5.4. In reality, wave information can be improved before the tuning procedure by fusion of wave data from multiple resources, such as from wave forecast, hindcast, onboard wave radar, visual observation, and nearby wave buoy measurements [33].

The algorithm contains several important parameters to tune, such as α, Q, R, and the initial P matrices. Experience suggests to apply a small α value (e.g., 0.1 or 0.01) for a better algorithmic performance. Normally, vessel heading and forward speed can vary slowly or be subjected to disturbance within a sea state. The process uncertainty Q should reflect how well the assumption about stationarity holds true in reality. Moreover, the vessel heading, forward speed, and inertia distribution can be frequently shifted depending on the operation scenarios (e.g., transportation, docking, and lifting). For such scenarios, control parameters should be introduced in the system propagation model. The measurement uncertainty R should in reality account for the possibly biased, non-Gaussian signal errors. It is also very important to filter the signal at the measurement update step in order to keep the vessel motion signals only in the wave frequency domain. It can be beneficial to initiate the vessel state covariance as being considerably larger than expected. Too small initial vessel state covariance indicates overconfidence in relation to the uncertain vessel parameters, leading to a too small Kalman gain K and thus slowing down the tuning towards convergence.
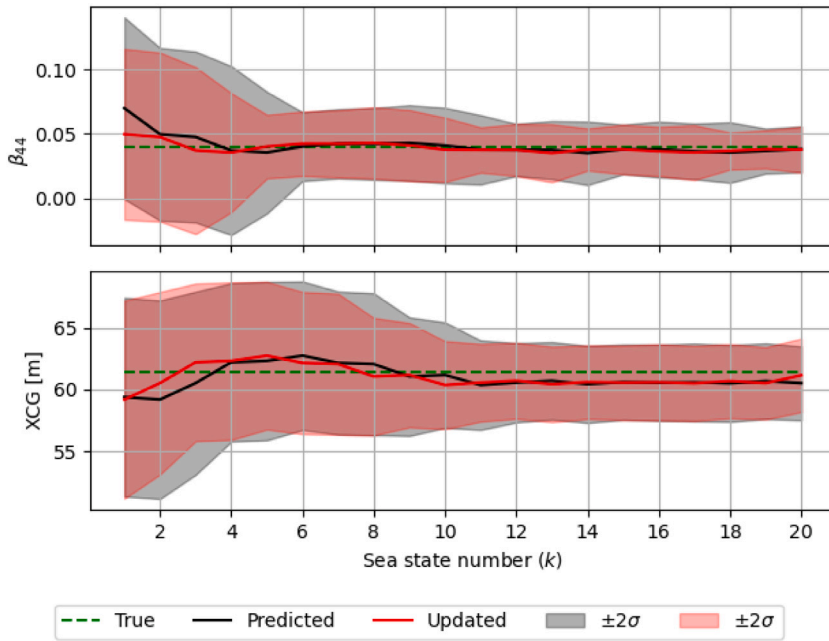
Fig. 15. The results of tuning β_{44} and XCG for the sensitivity study by using increasingly uncertain wave information with $\tau = 44$.
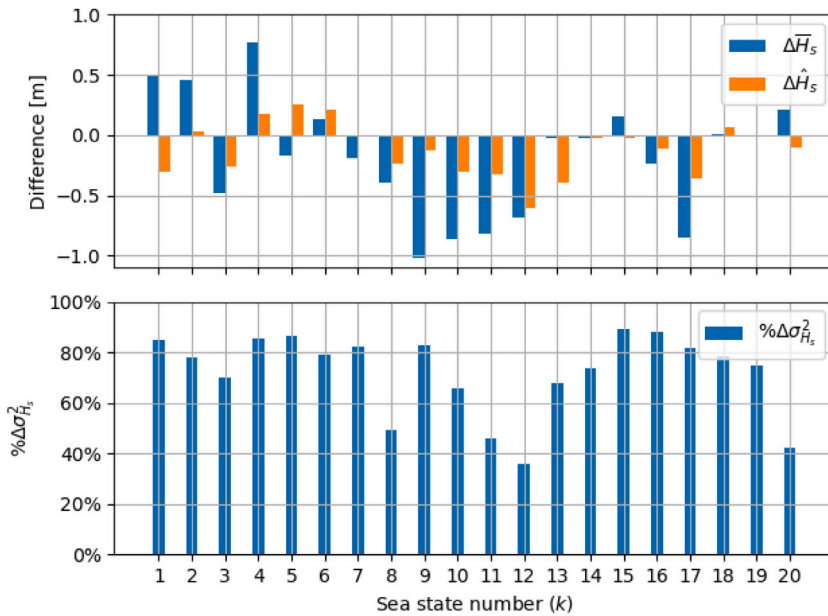

Fig. 16. Illustration of the errors before and after the tuning, and the variance reduction after tuning of H_s, for the sensitivity study by using increasingly uncertain wave information with $\tau = 44$.

The proposed algorithm is so flexible that the system state can basically include any uncertain parameters in relation to modeling of the linear potential theory based vessel seakeeping and description of sea state. A case study considering short-crested wave conditions with uncertain spreading parameter was also performed. As expected, the introduced uncertain spreading parameter n_s mainly affects the tuning of the wave direction related parameters such as β_W. n_s has very limited influence on tuning of the other sea state characteristics and vessel parameters simply because the wave direction related parameters influence the vessel motion measurements (i.e., the measurement space) differently from the other parameters.

In reality, a 2D wave spectrum with specified uncertainties in relation to each frequency component for each direction could be considered. The wave information uncertainties may be unbiased in the long term, whereas, these errors could be biased in the short
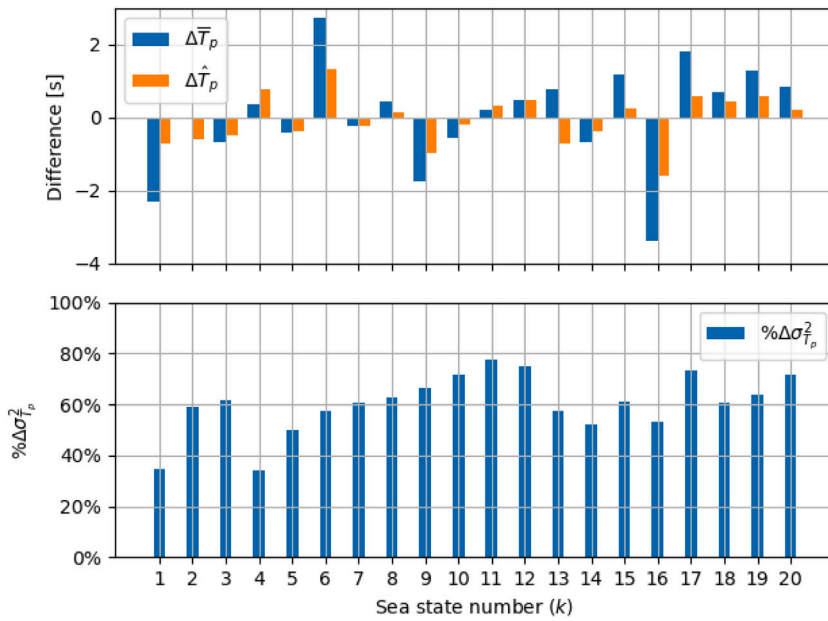
Fig. 17. Illustration of the errors before and after the tuning, and the variance reduction after tuning of T_p, for the sensitivity study by using increasingly uncertain wave information with $\tau = 44$.
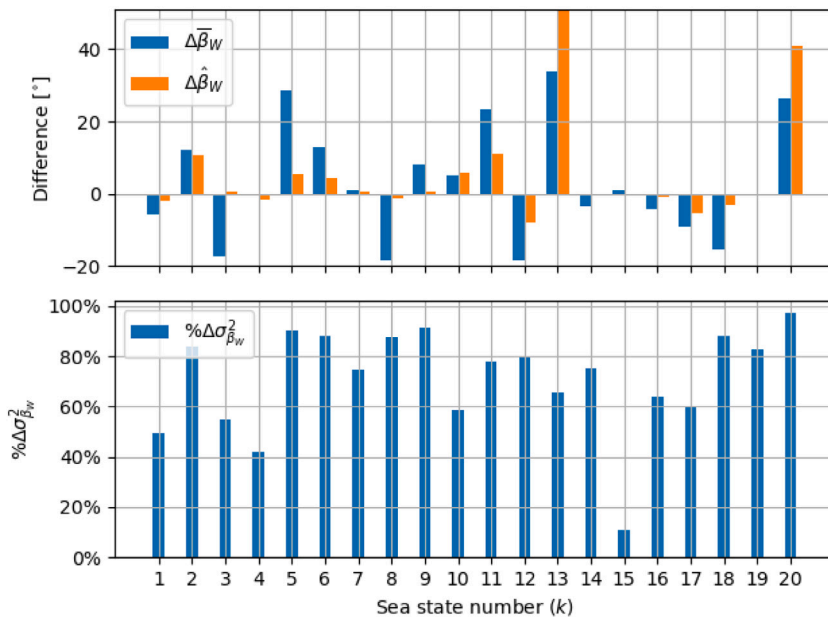

Fig. 18. Illustration of the errors before and after the tuning, and the variance reduction after tuning of β_W, for the sensitivity study by using increasingly uncertain wave information with $\tau = 44$.

term. This may therefore lead to divergent tuning results. The tuning model should, to a certain degree, tolerate those uncertainties, which might be challenging.

In reality, several other uncertain parameters should be considered including the vessel forward speed. Consequently, handling the response spectrum based on the encountered frequencies may become a challenge due to the well-known 3-to-1 mapping issue for following seas. The surface current, acting on the vessel as an additional "vessel speed", could also influence many important hydrodynamic coefficients such as damping and added mass. The measurements of surface current suffer from large uncertainties partly due to the influence from surface waves, the types and set-ups of instruments, and variation of the instrument quality for measuring current speed [35,54].

The vessel parameters related to inertia distribution and even geometry are time-variant in the long term. The real system should be able to detect the possible change of e.g., the vessel loading condition, and adaptively adjust the state accordingly. For example, this could be triggered when any of the updated vessel parameters is outside of its $\pm 3\sigma$ range.

So far, a constant value of the additional roll damping coefficient β_{44} for all sea states has been considered in the proposed UKF based tuning algorithm and the case studies. However, in reality β_{44} is sea state dependent. Han et al. [28] proposed an algorithm for tuning and prediction of sea state dependent roll damping, by application of discrete Bayesian inference with a surrogate model of roll damping. However, the procedure for the tuning of sea state dependent parameters is not straight forward for the proposed UKF based tuning algorithm. Tuning and predicting sea state dependent vessel parameters together with other uncertain parameters for the proposed UKF model considering uncertain wave information should be addressed in the future. Furthermore, the proposed algorithm should be validated by scaled tests and on-site measurement data.

It is also worth mentioning that the proposed UKF based tuning is an online algorithm. Since the vessel condition (in terms of vessel geometry, inertia distribution, etc.) typically does not change for a considerable period of time (e.g., few hours or days), the tuned vessel parameters and the corresponding vessel motion RAOs can therefore be applied to improve the prediction accuracy of vessel motions for real-time applications. However, vessel loading conditions can vary continuously and significantly during many critical marine operations, such as heavy lift and pipe laying. Consequently, the tuned vessel parameters based on available data before such operations may not be suitable to apply directly. Future research should consider how to tune and predict the vessel parameters, and consequently improve the prediction accuracy of critical responses during such non-stationary operations.

Declaration of competing interest

The authors declare that they have no known competing financial interests or personal relationships that could have appeared to influence the work reported in this paper.

Acknowledgments

References

[1] Tellkamp J, Bruns A, Gosch T, Günther H, Hansen PF, Nielsen UD, Papanikolaou A, Spanos D, Papatzanakis G, Kassner S, Wittkuhn D, Tränkmann I, Ehrke K-C, Krüger S, Vorhoelter H, Kluwe F, Jaap Struijk JKN. ADOPT summary of experiences and needs for further development. Technical report, FORCE Technology and Uniresearch; 2009.

[2] Han X, Sævik S, Leira BJ. A sensitivity study of vessel hydrodynamic model parameters. In: Proceedings of the ASME 2020 39th international conference on ocean, offshore and arctic engineering, Vol. 1. Virtual, Online; 2020, http://dx.doi.org/10.1115/OMAE2020-19039.

[3] Journée J, Pinkster J. Introduction in ship hydromechanics. Technical report, Delft University of Technology; 2002.

[4] Li G, Kawan B, Wang H, Zhang H. Neural-network-based modelling and analysis for time series prediction of ship motion. Ship Technol Res 2017;64(1):30–9. http://dx.doi.org/10.1080/09377255.2017.1309786.

[5] Kawan B, Wang H, Li G, Chhantyal K. Data-driven modeling of ship motion prediction based on support vector regression. In *Proceedings of the 58th conference on simulation and modelling (SIMS 58)*, 2017.

[6] Zhang W, Liu Z. Real-time ship motion prediction based on time delay wavelet neural network. J Appl Math 2014.

[7] Zhao X, Xu R, Kwan C. Ship-motion prediction: Algorithms and simulation results. In: 2004 IEEE international conference on acoustics, speech, and signal processing, Vol. 5. IEEE; 2004, p. V–125.

[8] Nielsen UD, Brodtkorb AH, Jensen JJ. Response predictions using the observed autocorrelation function. Mar Struct 2018;58:31–52. http://dx.doi.org/10.1016/j.marstruc.2017.10.012.

[9] DNVGL-ST-N001. Marine operations and marine warranty. Technical report, DNV GL; 2016.

[10] Faltinsen OM. Sea loads on ships and offshore structures. New York: Cambridge University Press Cambridge; 1990.

[11] Alford LK, Beck RF, Johnson JT, Lyzenga D, Nwogu O, Zundel A. A real-time system for forecasting extreme waves and vessel motions. International conference on offshore mechanics and arctic engineering, Volume 11: Prof. Robert F. Beck Honoring Symposium on Marine Hydrodynamics, 2015, http://dx.doi.org/10.1115/OMAE2015-42420.

[12] Connell BSH, Rudzinsky JP, Brundick CS, Milewski WM, Kusters JG, Farquharson G. Development of an environmental and ship motion forecasting system. In: International conference on offshore mechanics and arctic engineering, Volume 11: Prof. Robert F. Beck Honoring Symposium on Marine Hydrodynamics, 2015, http://dx.doi.org/10.1115/OMAE2015-42422.

[13] Stredulinsky DC, Thornhill EM. Ship motion and wave radar data fusion for shipboard wave measurement. J Ship Res 2011;55:73–85.

[14] Naaijen P, Roozen DK, Huijsmans RHM. Reducing operational risks by on-board phase resolved prediction of wave induced ship motions. International conference on offshore mechanics and arctic engineering, Volume 7: Ocean Engineering, 2016, http://dx.doi.org/10.1115/OMAE2016-54591.

[15] Hilmer T, Thornhill E. Deterministic wave predictions from the WaMoS II. In: OCEANS 2014 - taipei. 2014, p. 1–8. http://dx.doi.org/10.1109/OCEANS-TAIPEI.2014.6964526.

[16] Nielsen UD. A concise account of techniques available for shipboard sea state estimation. Ocean Eng 2017;129:352–62. http://dx.doi.org/10.1016/j.oceaneng.2016.11.035.

[17] Ren Z, Han X, Verma AS, Dirdal JA, Skjetne R. Sea state estimation based on vessel motion responses: Improved smoothness and robustness using Bézier surface and L1 optimization. Mar Struct 2021;76:102904. http://dx.doi.org/10.1016/j.marstruc.2020.102904.

[18] Galvin J. The use of information technology at the Met Office. British Computer Society, Bristol Branch January Seminar; 2014.

[19] Gusdal Y, Carrasco A, Furevik BR, Sætra Ø. Validation of the operational wave model WAM at met.no - report 2010. Technical report, Oslo: Norwegian Meteorological Institute; 2011.

[20] Hersbach H, Bell B, Berrisford P, Hirahara S, Horányi A, Muñoz Sabater J, Nicolas J, Peubey C, Radu R, Schepers D, Simmons A, Soci C, Abdalla S, Abellan X, Balsamo G, Bechtold P, Biavati G, Bidlot J, Bonavita M, De Chiara G, Dahlgren P, Dee D, Diamantakis M, Dragani R, Flemming J, Forbes R, Fuentes M, Geer A, Haimberger L, Healy S, Hogan RJ, Hólm E, Janisková M, Keeley S, Laloyaux P, Lopez P, Lupu C, Radnoti G, de Rosnay P, Rozum I, Vamborg F, Villaume S, Thépaut J-N. The ERA5 global reanalysis. Q J R Meteorol Soc 2020;146(730):1999–2049. http://dx.doi.org/10.1002/qj.3803, URL: https://rmets.onlinelibrary.wiley.com/doi/abs/10.1002/qj.3803 arXiv:https://rmets.onlinelibrary.wiley.com/doi/pdf/10.1002/qj.3803.
[21] Xu H, Hassani V, Guedes Soares C. Uncertainty analysis of the hydrodynamic coefficients estimation of a nonlinear manoeuvring model based on planar motion mechanism tests. Ocean Eng 2019;173:450–9. http://dx.doi.org/10.1016/j.oceaneng.2018.12.075.
[22] Xu H, Guedes Soares C. Hydrodynamic coefficient estimation for ship manoeuvring in shallow water using an optimal truncated LS-SVM. Ocean Eng 2019;191:106488.
[23] Yuan Y, Fu G, Zhang W. Extended and unscented Kalman filters for parameter estimation of a hydrodynamic model of vessel. In: 2016 35th chinese control conference (CCC). 2016, p. 2051–6.
[24] Fossen T, Sagatun S, SØrensen A. Identification of dynamically positioned ships. Control Eng Pract 1996;4(3):369–76. http://dx.doi.org/10.1016/0967-0661(96)00014-7.
[25] Han X, Leira BJ, Sævik S. Vessel hydrodynamic model tuning by discrete Bayesian updating using simulated onboard sensor data. Ocean Eng 2021;220. http://dx.doi.org/10.1016/j.oceaneng.2020.108407.
[26] ITTC. Recommended procedures and guidelines: Numerical estimation of roll damping. Technical report, International Towing Tank Conference; 2011.
[27] Kaplan P. Lecture notes on nonlinear theory of ship roll motion in a random seaway. 1966.
[28] Han X, Sævik S, Leira BJ. Tuning of vessel parameters including sea state dependent roll damping. Ocean Eng 2021. Revision under review.
[29] Gelman A, Carlin J, Stern H, Dunson D, Vehtari A, Rubin D. Bayesian data analysis. 3rd ed.. 2013.
[30] ECMWF. Part VII: ECMWF wave model. IFS documentation, vol. 7, ECMWF; 2016, URL: https://www.ecmwf.int/node/16651.
[31] Carrasco A, Saetra Ø. A limited-area wave ensemble prediction system for the Nordic Seas and the North Sea. Technical report, Oslo: Norwegian Meteorological Institute; 2008.
[32] ECMWF. Part V: Ensemble prediction system. IFS documentation, vol. 5, ECMWF; 2016, URL: https://www.ecmwf.int/node/16649.
[33] Natskår A, Moan T, Alvær P. Uncertainty in forecasted environmental conditions for reliability analyses of marine operations. Ocean Eng 2015;108:636–47.
[34] Orimolade AP, Furevik BR, Gudmestad OT. A comparison of wave height forecasts against wave measurements for a location in the barents sea and in the norwegian sea. In: Proceedings of the twenty-sixth (2016) international ocean and polar engineering conference. International Society of Offshore and Polar Engineers; 2016.
[35] Hagen Ø, Bitner-Gregersen EM, Vrouwenvelder A. JCSS probabilistic model code part 2: loads 2.15: wave loads. Technical report, Joint Committee on Structural Safety; 2006.
[36] World Meteorological Organization (2014). WMO guide to meteorological instruments and methods of observation. 2014.
[37] Reichert K, Hessner K, Nieto Borge JC, Dittmer J. WaMoS II: A radar based wave and current monitoring system. In: The Proceedings of the 9th (1999) International Offshore and Polar Engineering Conference. Brest, France: International Society of Offshore and Polar Engineers; 1999.
[38] Hersbach H, Bell B, Berrisford P, Biavati G, Horányi A, Muñoz Sabater J, Nicolas J, Peubey C, Radu R, Rozum I, Schepers D, Simmons A, Soci C, Dee D, Thépaut J-N. ERA5 hourly data on single levels from 1979 to present. 2021, http://dx.doi.org/10.24381/cds.adbb2d47, Copernicus Climate Change Service (C3S) Climate Data Store (CDS). Accessed on < 02-01-2021 >.
[39] ECMWF. Part II: Data assimilation. IFS documentation, vol. 2, ECMWF; 2016, URL: https://www.ecmwf.int/node/16666.
[40] ECMWF. Part I: Observations. IFS documentation, vol. 1, ECMWF; 2016, URL: https://www.ecmwf.int/node/16646.
[41] Bitner-Gregersen EM, Hagen Ø. Uncertainties in data for the offshore environment. Struct Saf 1990;7(1):11–34. http://dx.doi.org/10.1016/0167-4730(90)90010-M.
[42] DNVGL-RP-C205. Environmental conditions and environmental loads. Technical report, DNV GL; 2017.
[43] Labbe R. Kalman and bayesian filters in python. 2018, https://github.com/rlabbe/Kalman-and-Bayesian-Filters-in-Python.
[44] Van Der Merwe R, et al. Sigma-point Kalman filters for probabilistic inference in dynamic state-space models (Ph.D. thesis), OGI School of Science & Engineering at OHSU; 2004.
[45] Julier SJ, Uhlmann JK. New extension of the Kalman filter to nonlinear systems. In: Signal processing, sensor fusion, and target recognition VI. vol. 3068, International Society for Optics and Photonics; 1997, p. 182–93.
[46] Julier SJ. The scaled unscented transformation. In: Proceedings of the 2002 american control conference (IEEE Cat. No. CH37301), Vol. 6. IEEE; 2002, p. 4555–9.
[47] Nørgaard M, Poulsen NK, Ravn O. New developments in state estimation for nonlinear systems. Automatica 2000;36(11):1627–38. http://dx.doi.org/10.1016/S0005-1098(00)00089-3.
[48] Julier SJ, Uhlmann JK. A general method for approximating nonlinear transformations of probability distributions. Citeseer; 1996.
[49] Julier S, Uhlmann J, Durrant-Whyte HF. A new method for the nonlinear transformation of means and covariances in filters and estimators. IEEE Trans Automat Control 2000;45(3):477–82.
[50] DNV GL. Wasim user manual. Technical report, DNV GL; 2018.
[51] Lewandowski EM. The dynamics of marine craft: maneuvering and seakeeping, Vol. 22. World scientific; 2004.
[52] Nessim MA, Hong HP, Jordaan IJ. Environmental load uncertainties for offshore structures. Journal of Offshore Mechanics and Arctic Engineering 1995;117(4):245–51. http://dx.doi.org/10.1115/1.2827230.
[53] Jefferys E. Directional seas should be ergodic. Appl Ocean Res 1987;9(4):186–91. http://dx.doi.org/10.1016/0141-1187(87)90001-0, URL: http://www.sciencedirect.com/science/article/pii/0141118787900010.
[54] Bruserud K, Haver S. Uncertainties in current measurements in the northern north sea. J Atmos Ocean Technol 2017;34(4):855–76. http://dx.doi.org/10.1175/JTECH-D-16-0192.1.